Thesis

TECHNICAL UNIVERSITY OF CRETE
SCHOOL OF ELECTRICAL AND
COMPUTER ENGINEERING

Magnetoencephalogram analysis of subjects with mild head injuries using multilevel connectivity networks and graph neural networks

Sotiris Kavvouras

Committee

Professor Michail Zervakis
Professor Thrasyvoulos Spyropoulos
Professor Dionysios Christopoulos

Chania, March 2024

Credits

I would like to express my gratitude to the Technical University of Crete for its excellent support and resources, which contributed to the completion of this thesis.

Moving on, I would like to mention that my family's encouragement and belief in my abilities have been the cornerstone of my journey. Their support provided the emotional foundation that allowed me to meet the challenges of this endeavor. Subsequently, the collaboration, insightful comments and support of my friends not only enriched my research, but also inspired my journey with shared growth and camaraderie. I thank each one of them individually for their help over the years throughout my endeavor.

Finally, I would also like to thank my thesis supervisor, Professor Michael Zervakis, and my co-supervisor, Dr. Marios Antonakakis, for their constant presence and trust throughout this thesis, as well as for their advice on both the thesis and my future career. I would also like to thank Professor Michael Lagoudakis for our cooperation throughout the years of my studies (academic and otherwise), for the stimuli I received from him and for his guidance.

This thesis is a testament to the harmonious contribution of my family, friends, mentors, and my efforts.

Abstract

Mild Traumatic Brain Injury (mTBI) is a common neurological condition with significant cognitive and functional implications. This thesis presents a comprehensive investigation into the neural alterations associated with mTBI by employing advanced neuroimaging techniques and machine learning. Specifically, we employ Multi-Layer Functional Connectivity (MLFC) analysis, Machine Learning (ML), and Graph Neural Networks (GNNs) to unravel the intricate patterns of brain network disruption and provide insights into the underlying neurophysiological mechanisms. Magnetoencephalographic (MEG) recordings were acquired from mTBI patients and healthy controls during resting states. MLFC captures multi-layer correlations in different frequency bands, revealing subtle connectivity changes between brain regions. ML classification demonstrates the potential to discern mTBI patients from controls based on neural features. GNNs model brain regions as a graph, capturing complex interactions and non-linear relationships. Integrating GNNs enhances our understanding of mTBI-related disruptions, providing a more holistic perspective. Our study enhances insights into altered functional connectivity in mTBI patients. Although GNNs exhibit significantly superior performance compared to traditional machine learning methods, achieving an accuracy of approximately 97% versus 80-85%, the application of MLFC presents less definitive outcomes, with results appearing notably ambiguous, ranging between 50% and 65%. The fusion of MLFC, ML, and GNNs unveils nuanced dynamics not captured by traditional methods. These findings contribute to understanding mTBI pathophysiology and may guide personalized interventions.

Keywords: Mild Traumatic Brain Injury, Magnetoencephalography, Multi-Layer Functional Connectivity, Machine Learning, Graph Neural Networks, Neuroimaging, Brain Network Analysis.

Περίληψη

Η ήπια κρανιοεγκεφαλική κάκωση (mTBI) είναι μια συχνή νευρολογική πάθηση με σημαντικές γνωστικές και λειτουργικές επιπτώσεις. Η παρούσα διατριβή παρουσιάζει μια ολοκληρωμένη διερεύνηση των νευρωνικών μεταβολών που σχετίζονται με το mTBI με τη χρήση προηγμένων τεχνικών νευροαπεικόνισης και μηχανικής μάθησης. Συγκεκριμένα, χρησιμοποιούμε την ανάλυση της λειτουργικής συνδεσιμότητας πολλαπλών επιπέδων (MLFC), τη μηχανική μάθηση (ML) και τα νευρωνικά δίκτυα γράφων (GNN) για να διαλευκάνουμε τα περίπλοκα μοτίβα της διαταραχής των εγκεφαλικών δικτύων και να παράσχουμε πληροφορίες για τους υποκείμενους νευροφυσιολογικούς μηχανισμούς. Οι μαγνητοεγκεφαλογραφικές (MEG) καταγραφές αποκτήθηκαν από ασθενείς με mTBI και υγιείς μάρτυρες κατά τη διάρκεια καταστάσεων ηρεμίας. Η MLFC καταγράφει πολυεπίπεδες συσχετίσεις σε διάφορες ζώνες συχνοτήτων, αποκαλύπτοντας λεπτές αλλαγές στη συνδεσιμότητα μεταξύ των διάφορων περιοχών του εγκεφάλου. Η ταξινόμηση με τη χρήση της ML αποδεικνύει τη δυνατότητα διάκρισης των ασθενών mTBI από τους υγιείς με βάση τα νευρικά χαρακτηριστικά. Τα GNN μοντελοποιούν τις περιοχές του εγκεφάλου ως γράφο, αποτυπώνοντας πολύπλοκες αλληλεπιδράσεις και μη γραμμικές σχέσεις. Η ενσωμάτωση των GNN ενισχύει την κατανόηση των διαταραχών που σχετίζονται με το mTBI, παρέχοντας μια πιο ολιστική προοπτική. Αν και τα GNN παρουσιάζουν σημαντικά ανώτερες επιδόσεις σε σύγκριση με τις παραδοσιακές μεθόδους μηχανικής μάθησης, επιτυγχάνοντας ακρίβεια περίπου 97% έναντι 80-85%, η εφαρμογή της MLFC παρουσιάζει λιγότερο σαφή αποτελέσματα, με τα αυτά να εμφανίζονται ιδιαίτερα διφορούμενα, κυμαινόμενα μεταξύ 50% και 65%. Η μελέτη μας ενισχύει τις γνώσεις σχετικά με την τροποποιημένη λειτουργική συνδεσιμότητα σε ασθενείς με mTBI. Η συγχώνευση των MLFC, ML και GNN αποκαλύπτει αποχρώσεις της δυναμικής που δεν καταγράφονται από τις παραδοσιακές μεθόδους. Τα ευρήματα αυτά συμβάλλουν στην κατανόηση της παθοφυσιολογίας του mTBI και μπορούν να καθοδηγήσουν εξατομικευμένες παρεμβάσεις.

Λέξεις-κλειδιά: Ήπια Τραυματική Εγκεφαλική Κάκωση, Μαγνητοεγκεφαλογραφία, Λειτουργική Συνδεσιμότητα πολλαπλών Επιπέδων, Μηχανική Μάθηση, Νευρωνικά Δίκτυα γραφημάτων, Νευροαπεικόνιση, Ανάλυση Δικτύου Εγκεφάλου.

Contents

1. Introduction

The intricate workings of the human brain, its vulnerability in Mild Traumatic Brain Injury (mTBI), and the revelation of brain dynamics through Magnetoencephalography (MEG) signals form the crux of this thesis. As we unravel these components, the concept of functional connectivity emerges, offering a glimpse into the orchestration of neural networks. This introduction lays the groundwork for a journey into the depths of neuroscience, investigating the complex interplay that shapes our cognitive world.

1.1 Motivation

Mild traumatic head injuries (mTBI) are an understudied area despite their potential long-term impact on brain function. In recent years, advancements in neuroimaging techniques have provided unprecedented insights into the brain's intricacies. Among these, Magnetoencephalography (MEG) emerges as a powerful tool for capturing the dynamic neural activity with high temporal resolution. However, the analysis of MEG data in the context of mTBI remains relatively unexplored.

This research seeks to address this gap by focusing on the comprehensive analysis of MEG data from subjects with mild head injuries. The investigation revolves around the utilization of cutting-edge techniques, particularly multilevel connectivity networks and graph neural networks (GNNs), to unravel the hidden patterns and disruptions within the brain's functional connectivity. While some studies have explored functional connectivity alterations in mTBI, few have delved into the specific features that can optimally represent and handle the brain network as a graph.

The significance of this research lies in its potential to shed light on the intricate dynamics of brain networks following mTBI, offering insights into the mechanisms of injury and recovery. By employing multilevel connectivity networks, we aim to uncover nuanced alterations across different connectivity layers, elucidating the temporal and frequency-specific changes in neural communication.

Additionally, the integration of GNNs presents an exciting avenue to capture the non-linear relationships between brain regions, providing a holistic understanding of how these disruptions cascade through the network.

Existing studies have primarily focused on broad connectivity changes or single-layer analysis, lacking the granularity that multilevel networks and GNNs can offer. Our research aims to bridge this gap, unraveling intricate connectivity patterns that could potentially serve as diagnostic and prognostic markers for mTBI. Moreover, the exploration of brain network representation and handling as a map through these advanced techniques opens new avenues for understanding the spatial and temporal dynamics of brain network alterations.

In conclusion, this research embarks on a journey to explore the uncharted territory of mTBI using MEG data analysis through multilevel connectivity networks and GNNs. The outcomes have the potential to revolutionize our understanding of mTBI-related brain network disruptions, providing crucial insights for both clinical assessment and potential interventions. This endeavor represents a pioneering effort in unraveling the complexities of brain connectivity in the aftermath of mild head injuries, offering a fresh perspective on the representation and handling of brain networks as intricate maps of neural communication.

1.2 Contribution

The primary thrust of this thesis rests upon the transformative insights gleaned from the novel perspective of treating the brain's functional connectivity network as a graph. This paradigm shift has rendered a substantial contribution to the field, imparting a holistic perspective on the intricacies of functional connectivity. The integration of graph classification methodologies has imbued our research with a comprehensive understanding of the underlying features embedded within the functional connectivity map. By delving into detailed timeseries emanating from each Region of Interest (ROI),

which encompasses quantified connections, temporal and frequency-based features, as well as graph properties, our approach has demonstrated superior performance in yielding more accurate results.

Moreover, an additional noteworthy contribution stems from the comprehensive comparison and evaluation of multiple functional connectivity estimators. The exploration of Mutual Information, imaginary Phase Locking Value, and Amplitude Envelope Correlation in conjunction with the two distinctive topologies (2D data representation and graph representation) has served as a testament to the versatility of our research. Such a comprehensive comparison enables a comprehensive assessment of the strengths and limitations of each estimator within distinct contexts. Further enriching this comparative analysis, we have meticulously evaluated the performance of six classifiers across these diverse representations and topologies. This encompassing approach spans three classifiers dedicated to the 2D data representation and an equivalent number for the graph representation, inclusive of Neural Networks for both categories.

In conclusion, this thesis stands as a testament to the power of innovative perspectives and comprehensive evaluations. The pivotal shift in considering the brain's functional connectivity as a graph has not only expanded our understanding of brain network dynamics but has also opened avenues for more accurate and nuanced insights. The comprehensive exploration of various functional connectivity estimators, coupled with the exhaustive comparison of data representations and classifiers, reinforces the robustness of our findings, and enhances the broader understanding of functional connectivity analysis techniques. Through these substantial contributions, this research has paved the way for a more sophisticated and nuanced approach to the study of brain network dynamics and their implications for various neuroscientific and clinical applications.

1.3 Structure

Chapter 2 delves into the foundational knowledge necessary for comprehending the subsequent research. The intricate structure and functioning of the human brain are explored, elucidating the complexities underlying neural dynamics. An in-depth understanding of Mild Traumatic Brain Injury (mTBI) is provided, shedding light on the implications of such injuries. Additionally, the principles of Magnetoencephalography (MEG) are expounded upon, showcasing its relevance as a neuroimaging technique. The chapter concludes with a thorough exploration of functional connectivity, elucidating its role in unraveling brain network interactions.

In **Chapter 3**, the methodology employed in preparing the data for analysis is intricately detailed. The various steps of data preprocessing applied to MEG data are meticulously explained, ensuring the integrity of the subsequent analyses. The construction of single-layer functional connectivity networks is comprehensively discussed, laying the foundation for subsequent network modeling. The chapter extends the exploration to multi-level functional connectivity networks, capturing temporal and frequency-specific nuances. The shift from traditional network representations to the innovative graph-based modeling of the brain is introduced.

The focal point of **Chapter 4** is the elucidation of diverse classification methods employed in the research. A comprehensive introduction to Convolutional Neural Networks (CNNs) is provided, along with their tailored application in the analysis of brain networks. The discussion further encompasses the significance of Graph Convolutional Networks (GCNs) in handling graph-based data derived from brain networks. Moreover, the principles of Support Vector Machines (SVMs) and k Nearest Neighbors (k-NN) are expounded upon, highlighting their relevance in classification tasks.

Finally, **Chapter 5** unveils the empirical outcomes obtained from the implemented classification methods. The presentation of results is structured to facilitate a comprehensive understanding of performance across different methods and network representations. The findings are critically

compared and interpreted in alignment with the research objectives. The chapter further engages in an insightful discussion, elucidating the implications of the results within the broader context of brain network analysis. In this Chapter, also, the research extends into future possibilities and potential avenues for exploration. The chapter identifies areas for further research, addressing unresolved questions and limitations encountered during the study.

2. Fundamentals

2.1 Anatomy and Physiology of the Brain

The nervous system, an intricate network comprising diverse neural tissues, serves the purpose of transmitting information to regulate bodily activities and functions (Carr and Brown, 2001). Moreover, it empowers the body to detect and respond to environmental changes while interpreting ensuing nerve impulses. Based on anatomical and physiological criteria, the nervous system can be dichotomized into two systems (Carr and Brown, 2001; National Institute on Aging, 2008):

• The **Central Nervous System** (CNS): Constituting the largest component of the nervous system, it resides within the cranial and spinal cavities, safeguarded by the skull and spinal structures, respectively.

• The **Peripheral Nervous System** (PNS): Comprising nervous tissue that extends from or converges toward the cranial and spinal cavities, the PNS extends throughout the limbs and torso tissues.
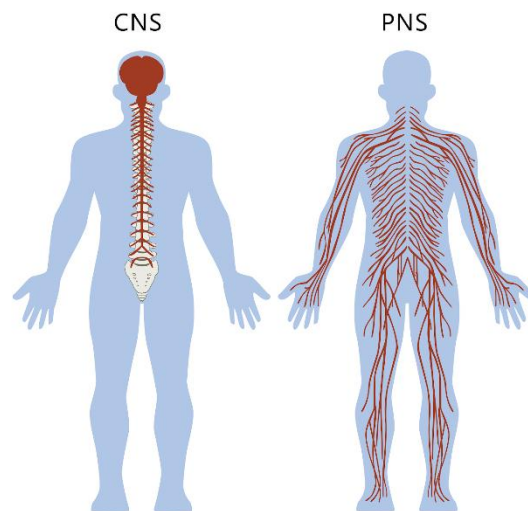
Figure 2.1 The Peripheral and the Central Nervous System from https://thepartnershipineducation.com/resources/nervous-system

The brain, constituting the largest portion of the central nervous system (CNS), encompasses several distinct structures. The cerebellum, situated atop the brain stem, is one such structure. The cerebrum, regarded as the most evolved component, is bifurcated into two cerebral hemispheres interconnected by the corpus callosum. Cloaking these hemispheres is the cortex, a pivotal arena for functions such as memory, attention, thought, and language, encompassing various cognitive functions. Notably, the

cortex's prominent fissures grant each hemisphere division into four lobes, each endowed with distinctive functions (National Institute on Aging, 2008):
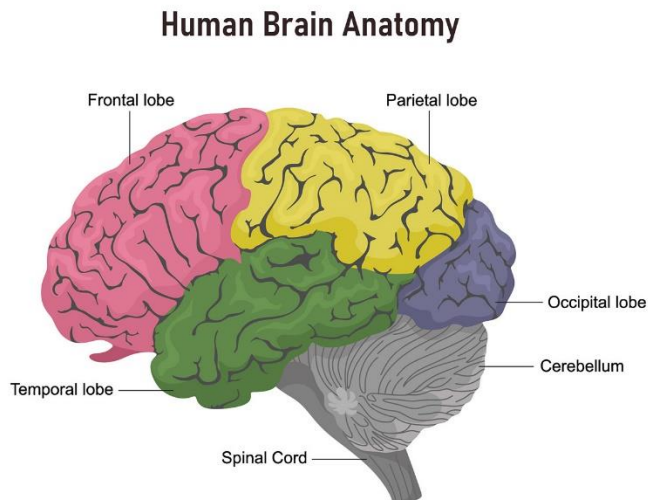

Figure 2.2 *The Anatomy of the Human Brain from* https://www.researchgate.net/figure/Four-Lobes-of-Human-Brain_fig1_377702102

- The **frontal lobe**, positioned at the brain's forefront, governs executive functions like planning, problem-solving, memory, attention, and movement.

- Positioned behind the frontal lobe, the **parietal lobe** orchestrates the perception and integration of sensory stimuli.

- Lining the brain's side beneath the frontal and parietal lobes, the **temporal lobe** governs the senses of smell, taste, and sound, alongside memory formation and storage.

- Nestled at the brain's rear, the **occipital lobe** is responsible for visual processing.

Comprising the CNS are glial and nerve cells, a fact underscored by Sanei and Chambers (2007). Positioned amidst neurons, glial cells fulfill a supportive role by anchoring and nurturing neurons with essential nutrients. Moreover, they facilitate the removal of damaged cells and debris while offering insulation to neurons. In contrast, the pivotal task of information transmission and processing within the nervous system is exclusively undertaken by neurons (National Institute on Aging, 2008).

A salient point is the EEG and MEG activity's derivation from the culmination of nerve impulse transmission or action potentials. These action potentials, temporary fluctuations in neuron membrane potential, travel along axons. Their initiation arises from ion exchanges across neuron membranes,

triggered by neurotransmitter chemical activity at synapses. The conduction velocity of these action potentials spans a range from 1 m/s to 100 m/s (Sanei and Chambers, 2007).

2.2 Mild Traumatic Brain Injuries (mTBI)

Mild traumatic brain injury (mTBI) stands as the prevailing cause of cerebral trauma. The mildest category within traumatic brain injury (TBI), mTBI, while qualifying as an acute cerebral injury, predominantly engenders short-lived physiological deviations without enduring neurological ramifications. The absence of lasting neurological deficits has led to the neuropsychological assertion that any cognitive or behavioral changes post-concussion lack permanent neuropathological underpinnings (Bigler, 2013). This assertion is predicated on the majority of mTBI sufferers returning to their pre-injury baseline and resuming normative functions, as corroborated by conventional neuropsychological metrics (Rohling et al., 2011). This outcome is supported by the notion that transient disturbances in neuronal physiology plausibly account for the positive outcomes frequently observed in mTBI investigations (Bigler, 2013).

Invariably, individuals undergoing mTBI experience a transient alteration in consciousness or mental state, followed by post-concussion symptoms (PCS) (Cassidy et al., 2004). Such symptoms, including headaches, fatigue, and dizziness, typically manifest on the day of injury and endure for several days thereafter (Boccaletti et al.,

Figure 2.3 Application of National Emergency X-Radiography Utilization Study (NEXUS) Head CT decision tool (NEXUS Head CT) to find roof of mTBI from https://www.acepnow.com/mtbi-resource-center/.

2006). For most patients, cognitive function recuperates, and PCS resolve within a three-month span. However, a subset of patients, up to 25% (Sigurdardottir et al., 2009), grapple with persisting PCS, long-term impairment, and potentially disability (Levin, 2009), thereby highlighting the crucial necessity of efficiently identifying mTBI-related alterations. A range of cognitive functions are impacted by mTBI, spanning attention (De Monte et al., 2006; Vanderploeg et al., 2005), working memory (Vanderploeg et al., 2005), episodic memory (Tsirka et al., 2011), verbal learning (De Monte et al., 2006; Ruff et al., 1989), and visual memory (Levin et al., 1987; Raskin, 2000; Ruff et al., 1989).

Traditional neuroimaging methods, such as magnetic resonance imaging (MRI) and computed tomography (CT), possess limited sensitivity to unveil the physiological shifts induced by mTBI (Bigler and Orrison, 2004; Johnston et al., 2001; Kirkwood et al., 2006). Conversely, contemporary neuroimaging techniques have highlighted that a subset of mTBI patients exhibit more than transient disruptions in neural function, evidencing identifiable underlying neuropathology (Bigler and Maxwell, 2012; Kasahara et al., 2012; Kim et al., 2013; Lewine et al., 2007; Lipton et al., 2012; Matthews et al., 2012; Wada et al., 2012). A distinct approach, magnetoencephalography (MEG), a noninvasive functional imaging method, directly measures neuronal currents within gray matter, featuring remarkable temporal resolution (<1 ms) and spatial localization precision (2–3 mm) (Leahy et al., 1998). Consequently, in recent years, numerous endeavors have sought to develop reliable mTBI biomarkers grounded in MEG data (explored in reviews by Jeter et al., 2013 and Huang et al., 2009, 2014). Noteworthy is the examination of resting-state MEG activity, either exclusively (Luo et al., 2013; Zouridakis et al., 2012; Dimitriadis et al., 2015; Li et al., 2015) or coupled with diffusion tensor imaging (DTI) MRI (Huang et al., 2014).

2.3 Magnetoencephalography (MEG)

Figure 2.4 *Process of MEG signals collection from* https://en.wikipedia.org/wiki/Magnetoencephalography.

Upon neuronal activation, synaptic currents arise within dendrites and propagate through the soma and axon. This generates a measurable magnetic field via MEG equipment and a secondary electrical field on the scalp via EEG equipment, typically within the frequency range below 70 Hz (Velmurugan, Sinha, and Satishchandra 2014). Notably, only when substantial populations of neurons simultaneously fire does a sufficiently robust signal emerge for scalp recording (Sanei and Chambers, 2007). The cortex autonomously generates electromagnetic activity composed of superimposed rhythms. Importantly, greater synchronization among neighboring neurons results in larger amplitude and lower frequency of the ensuing activity. Within healthy adults, signal amplitudes and frequencies shift between different human states such as wakefulness or sleep (Sanei and Chambers, 2007). These wave characteristics also transform with age. Typically, five major brain waves, each associated with a distinct frequency range, are discerned in brain activity: δ (0.5 Hz − 4 Hz), θ (4 Hz − 8 Hz), α (8 Hz − 13 Hz), β (13 Hz − 30 Hz), and γ (over 30 Hz) (Velmurugan, Sinha, and Satishchandra 2014).

The **δ** activity spans approximately 0.5 Hz to 4 Hz, primarily linked to deep sleep but also appearing in waking states. Occasionally, this activity might be confounded with artifact signals arising from neck and jaw muscles (Sanei and Chambers, 2007).

θ waves oscillate between 4 Hz and 8 Hz, associated with unconscious material access, creative inspiration, and deep meditation. Often co-occurring with other frequencies, θ waves seem correlated

with arousal levels. They play a crucial role in infancy and childhood, while significant θ activity in awake

adults can signify abnormalities (Sanei and Chambers, 2007). Changes in θ rhythms are also scrutinized

for emotional and maturational studies (Sanei and Chambers, 2007).

     α waves are prominent over the occipital brain region and lie within the 8 Hz to 13 Hz frequency

range. They typically manifest as sinusoidal or rounded signals (Sanei and Chambers, 2007). This rhythm

is associated with both relaxed awareness without focused attention and concentration. Predominantly

occurring when the eyes are closed, it's been theorized to represent a waiting or scanning pattern

stemming from visual brain regions. Opening eyes, encountering unfamiliar sounds, anxiety, or attention

significantly diminish α activity (Sanei and Chambers, 2007).

     β rhythm encapsulates brain electromagnetic activity oscillating between 13 Hz and 30 Hz. It

characterizes active thinking, attention, and problem-solving in the waking state (Sanei and Chambers,

2007). Common in the frontal and central regions of normal adults, β activity can also be elevated

around tumor regions (Sanei and Chambers, 2007).

     The **γ** range encompasses frequencies beyond 30 Hz, marked by low amplitude and rare

occurrence. Detecting such activity can provide confirmation of specific brain disorders (Sanei and

Chambers, 2007).

2.4 Functional Connectivity

     Research indicates that the human cerebral
cortex is comprised of distributed neural
assemblies, intricately linked, and interconnected to
create an extensive cortical circuit, resembling a
"web-like" arrangement (Varela et al. 2001;
Boccaletti et al. 2006; Schnitzler and Gross 2005;
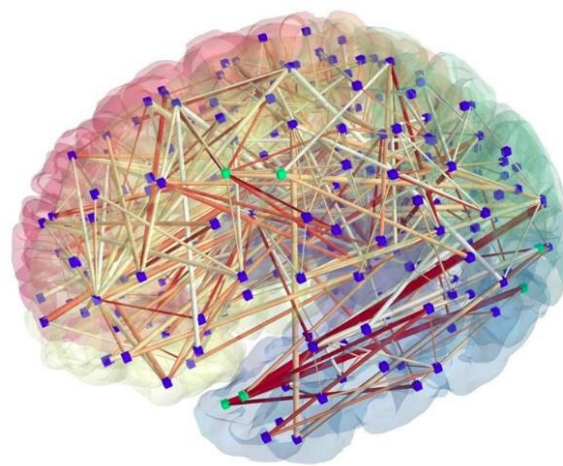
Figure 2.5 Functional Connectivity among neural nodes in a brain from https://computingforpsychologists.wordpress.com/tag/eeg/.

Carter, Shulman, and Corbetta 2012). Within this framework, connections are commonly described as either structural or functional in nature. In this thesis, we are going to focus on the functional connections.

2.4.1 Definition

Functional connectivity refers to the statistical dependencies between spatially distinct neurophysiological events within the brain. Unlike structural connectivity, which delineates the anatomical pathways between different brain regions, functional connectivity is concerned with the dynamic interactions that occur over time. It provides a quantitative measure of the co-activation or co-variation in neural activity between separate areas of the brain, offering a statistical representation of how these regions are functionally linked. Functional connectivity serves as a cornerstone for constructing and analyzing brain networks, enabling researchers to understand the complex interplay of neural circuits and their role in cognitive functions and behavioral outcomes.

Electroencephalography (EEG) and Magnetoencephalography (MEG) are neuroimaging techniques that offer more direct measures of neural activity compared to other methods like functional Magnetic Resonance Imaging (fMRI). MEG captures the magnetic fields produced by neural currents. These techniques are particularly valuable for studying functional connectivity because they provide a finer temporal resolution, allowing researchers to capture rapid fluctuations in neural activity that are often missed by other imaging methods (Nunez and Srinivasan, 2006; Hämäläinen et al., 1993).

Functional connectivity serves as the foundational framework for constructing brain networks. In this context, brain networks are often represented as graphs, where the nodes correspond to different brain regions and the edges signify functional connections between these regions. The strength and directionality of these connections are usually quantified through statistical measures, some of which are going to mentioned later (Friston, 1994; Bullmore & Sporns, 2009).

The topological properties of these brain networks can be further analyzed using graph theory. This mathematical approach provides a set of metrics, such as clustering coefficients, path lengths, and modularity, that offer insights into the organization, efficiency, and resilience of the brain's functional architecture (Rubinov & Sporns, 2010; Watts & Strogatz, 1998).

2.4.2 Functional Connectivity Estimators

Understanding the intricate web of functional connections within the brain requires robust and reliable estimators. These estimators quantify the strength and nature of the interactions between different neural populations, thereby providing insights into the brain's functional architecture. Among the plethora of estimators available, three have gained prominence for their efficacy and interpretability: Imaginary Phase Locking Value (iPLV), Mutual Information (MI), and Amplitude Envelope Correlation (AEC).

Imaginary Phase Locking Value. iPLV is a phase-based estimator that quantifies the consistency of the phase difference between two signals over time. Unlike its predecessor, the Phase Locking Value (PLV), iPLV mitigates the effects of volume conduction by focusing on the imaginary component of the cross-spectrum (Nolte et al., 2004; Palva & Palva, 2012). This makes iPLV a more reliable measure for true interactions between distinct neural sources. This estimator is computed as:

$$A_{XY}^{iPLV} = \left| \frac{1}{T} \sum_{t=1}^{T} Im\{e^{-i(\varphi_X(t) - \varphi_Y(t))}\} \right|,$$

where $\varphi(t) = \arctan\left(\frac{\tilde{x}(t)}{x(t)}\right)$ is the phase of a MEG signal at time t, whose analytical representation z of signal x is $z(t) = x(t) + i\tilde{x}(t)$, where i is the imaginary component and the $\tilde{x}(t)$ is the corresponding Hilbert transform.

Mutual Information. MI is a non-parametric estimator that captures both linear and nonlinear dependencies between two signals. It quantifies the amount of information that one signal can provide about another, making it a versatile tool for studying complex neural interactions (Cover & Thomas, 2006; Ince et al., 2017). The adjacency matrix using MI is calculated as:

$$A_{XY}^{MI} = \sum_{X_i, Y_j} P_{XY}(X_i, Y_j) log\left(\frac{P_{XY}(X_i, Y_j)}{P_X(X_i) P_Y(Y_j)}\right),$$

where P_{XY}, P_X and P_Y are the joint and marginal probability distributions, respectively.

Amplitude Envelope Correlation. AEC measures the correlation between the amplitude envelopes of two signals, often after filtering them into specific frequency bands. Unlike phase-based measures, AEC focuses on the amplitude dynamics, making it particularly useful for studying networks where power fluctuations are of interest (Brookes et al., 2011; Hipp et al., 2012). The adjacency matrix using AEC is given by:

$$A_{XY}^{AEC} = \left|\frac{\sum_t (x(t) - \bar{x})(y(t) - \bar{y})}{\sqrt{\sum_t (x(t) - \bar{x})^2} \sqrt{\sum_t (y(t) - \bar{y})^2}}\right|,$$

like Pearson's Correlation, but the x and y are the amplitudes of the respective signals computed using $amp(t) = \sqrt{x^2(t) + \tilde{x}^2(t)}$. $\bar{x}$ is the mean value of MEG signal x.

3. Data Preprocessing and Network Construction

In this chapter, we delve into the critical initial steps of data preprocessing and network construction, laying the groundwork for subsequent analyses of functional connectivity (FC) in brain networks. We begin by outlining the preprocessing techniques essential for ensuring data quality and reliability. Following this, we introduce both single and multi-level layer representations of FC brain networks, elucidating how these complex interactions can be quantified and understood. Finally, we discuss the transformation of these FC networks into graph form, a representation that enables sophisticated topological analyses. This chapter serves as a comprehensive guide for constructing and analyzing FC brain networks, setting the stage for further exploration and interpretation.

Figure 3.1 *MEG signals of a random sample generated by MNE python tool for neuro-signal processing.*

3.1 Subjects and Data features

The present research involved 30 right-handed individuals Healthy Controls (HC) (average age 29.25 ± 9.1 years) as well as 30 right-handed subjects with mild traumatic brain injuries (mTBI) (average age 29.33 ± 9.2 years). Written consent was obtained from all participants. Qualified clinicians reviewed and supplied all relevant clinical details, summarized in **Table 3.1**. The control group, sourced from

UTHSC-Houston's normative data repository, was specifically chosen to match the age of the mTBI group and had no history of head injuries, significant dental procedures, substance misuse, neurological or psychiatric conditions, or incompatible implants for MEG. The study was approved by institutional review boards and adhered to HIPAA guidelines.

Table 3.1 | *Patient Demographics for the mTBI group*

Age at injury (min—max)	Males (females)	Auto pedestrian— frontal (# subjects)	Auto pedestrian— frontal—type (# subjects)	Auto pedestrian— frontal—location (# subjects)
(19-25)	7(5)	Assault (2), Motor Vehicle (5), Sports-related (2), Auto Pedestrian (1), ATV (1), Assault (1)	Contusion (4), Bruising (3), Laceration—no sutures (1), Tenderness (2), Laceration—with sutures (2)	Head (10), Head/Face (2)
(25-40)	8(2)	Fall (1), Auto Pedestrian (2), Fall Moving Object (1), Assault (1), Motor Vehicle (1), Fall Raised Surface (2), Assault (1), Blow to Head (1)	Abrasion (3), Bruising (1), Tenderness (2), Contusion (3), Laceration—no sutures (1)	Head (9), Head/Face (1)
(40-50)	3(5)	Motor Vehicle (3), Assault (1), Fall Standing (2), Motorcycle (1), Fall Moving Object (1)	Abrasion (1), Bruising (1), Tenderness (4), Laceration—no sutures (1), Tenderness (1), Contusion (1), Laceration—with sutures (1)	Head (8)

The first column shows the age at injury as a range. The second column presents the number of genders separately. The rest of the columns indicate the type of injury while the number of patients is noticed within the parenthesis.

The mTBI participants were enlisted from three trauma centers in the greater Houston area, as part of a broader study (Zouridakis et al., 2012). Detailed information is available in previous publications (Zouridakis et al., 2012; Dimitriadis et al., 2015; Antonakakis et al., 2020). The mTBI patients were characterized according to the standards set by the American Congress of Rehabilitation Medicine (Kay et al., 1993) and the Department of Defense (Assistant Secretary, 2007).

Data was collected using a Magnes WH3600 system with 248 axial gradiometers (4D Neuroimaging Inc., San Diego, CA). The recording lasted for 10 minutes at a sampling rate of 1,017.25Hz, with an online bandpass filter between 0.1 and 200Hz to minimize noise. No separate eye or heart

activity was recorded. Participants lay supine with their eyes shut during the data collection. After removing artifact-contaminated activity (Dimitriadis et al., 2015) and converting the data to planar gradiometer field approximations using Fieldtrip (Oostenveld et al., 2011), approximately 5 minutes of clean data were retained for subsequent analysis.

3.2 Preprocessing

In this section, we will delve into the essential preliminary steps of signal preprocessing, a cornerstone in neuroimaging analysis. We will cover various artifact filtering techniques designed to improve signal quality and reliability. Source analysis methods for pinpointing neural activity will also be discussed. Additionally, we will introduce spectrum decomposition, a critical process for isolating specific frequency bands that are relevant to brain function. The creation of adjacency matrices will be explored as well, serving as the foundational structure for representing functional brain connectivity. Finally, edge filtering techniques will be addressed, aimed at refining the network by removing extraneous connections.
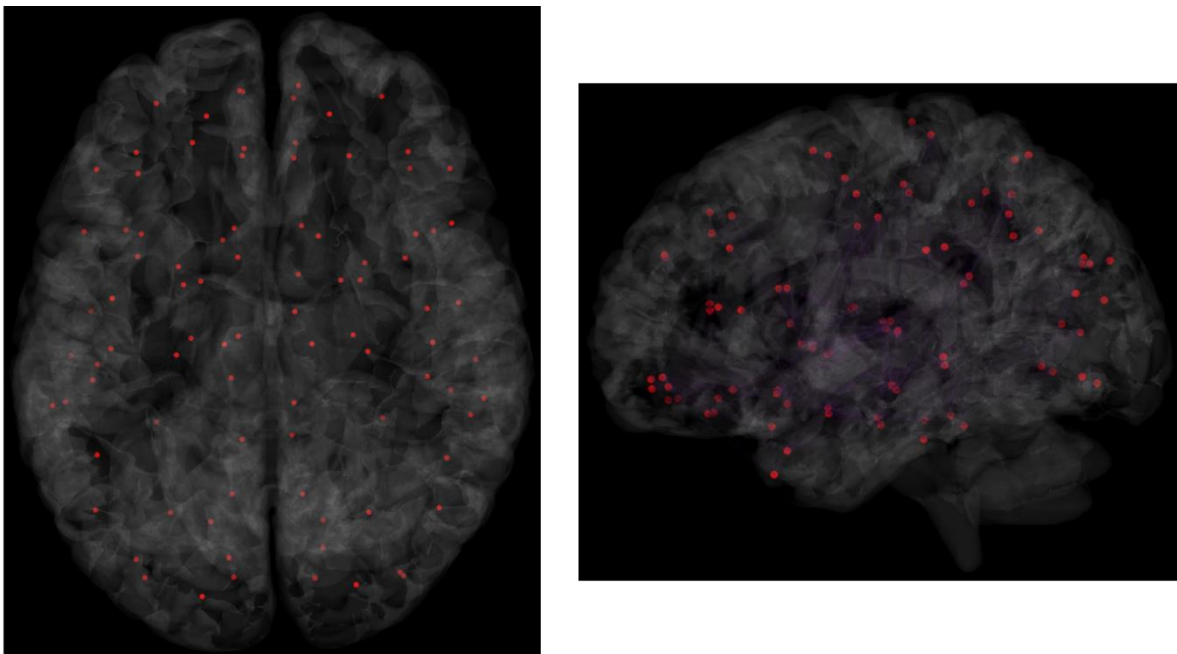

Figure 3.1. *Brain and the Regions of Interest from above and side view (picture created with visbrain).*

3.2.1 MEG Preprocessing and Source Analysis

In the thesis under discussion, the preprocessing of MEG signals was adapted from existing research methodologies (Antonakakis et al., 2020). Artifact minimization was accomplished through various techniques, including channel interpolation to rectify flawed channel activity, digital filtering to retain crucial frequency components, and the removal of white noise. Additionally, ocular, and cardiac artifacts were eliminated using Independent Component Analysis (ICA) algorithms.

For the analysis of neural sources, the study employed atlas-based beamforming to explore various frequency bands. The MRI anatomical regions were segmented into 90 distinct brain Regions of Interest (ROIs) using the Automated Anatomical Labeling (AAL) atlas as a reference. A spherical head model comprising 5,061 sources was utilized to encompass the entire brain tissue. The researchers then reconstructed MEG source activity using the Linearly Constrained Minimum Norm Variance (LCMV) algorithm. A representative source signal was determined for each ROI, and correlations between all possible pairs of source time series were calculated to construct a unified graph representing voxel temporal associations. Finally, a weighted sum of voxel time series was used to estimate a representative time series for each ROI.

3.2.2 Spectral Decomposition

Initially, the MEG signals from each participant were segregated into the targeted frequency bands, resulting in the generation of new signals corresponding to each frequency range—delta (δ, 0.5–4Hz), theta (θ, 4–8Hz), alpha (α, 8–13Hz), beta (β, 13–30Hz), and gamma (γ, 30–70Hz). A visual representation of this filtering process is provided in **Figure 3.2**. The filter used was a Butterworth passband filter of moving order (3 to 8) to acquire the most useful information on each band.
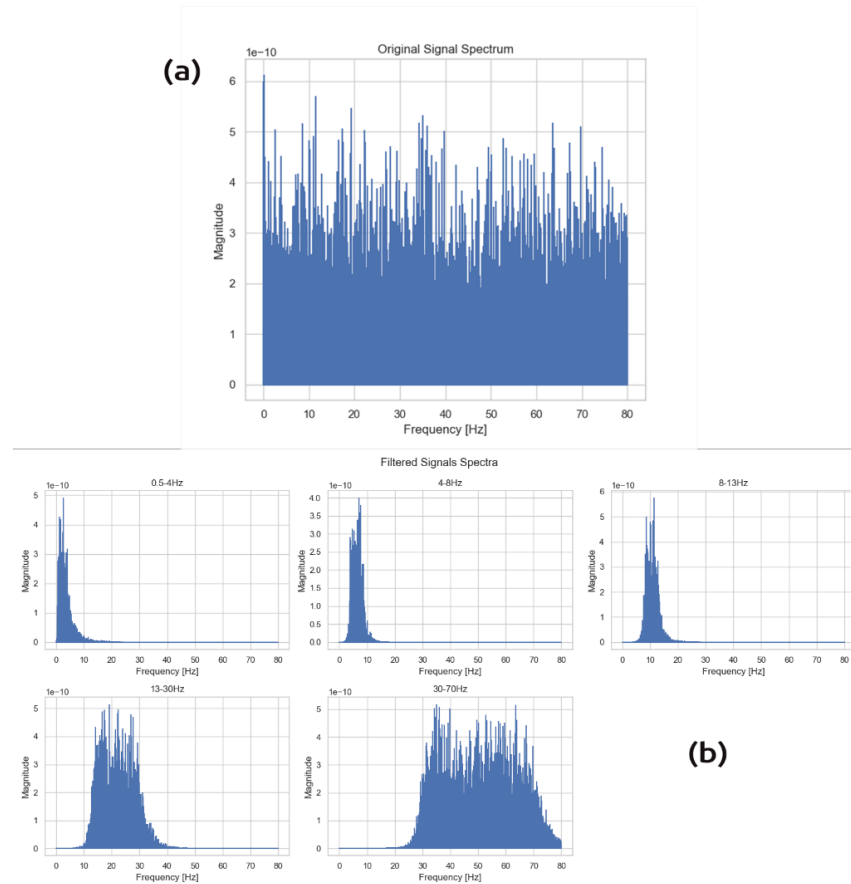
Figure 3.2. *(a) The power spectrum of a TBI patient's MEG signal, from the left Precentral gyrus of his brain. (b)The power spectrum of the same signal, filtered into the frequency bands (δ, ϑ, α, ß, γ).*

3.2.3 Adjacency Matrices

Following the filtering process, we advanced to the generation of functional connectivity maps. The functional connectivity maps, in fact, are represented as adjacency matrices. An adjacency matrix A = { w_{ij} } can be created to store the connectivity coefficients between each pair of Regions of Interest (ROIs). In this N x N matrix, N represents the total number of ROIs, and w_{ij} denotes the connectivity coefficient or the weight of the connection between ROI i and ROI j. These matrices were created for each frequency band—delta (δ), theta (θ), alpha (α), beta (β), and gamma (γ)—and for each functional connectivity estimator, namely IPLV, MI, and AEC. This was accomplished by applying the respective computational formulas of each estimator to the pairs of filtered signals for each participant. To

illustrate, we constructed the subsequent adjacency matrices, displayed in **Figure 3.3.1, Figure 3.3.2** and **Figure 3.3.3**. On the maps, each pixel represents the estimation of the connectivity between 2 signals coming from 2 ROIs. The diagonal elements of each matrix is set to 0, to exclude self-connections and to focus only on the interactions between different signals.
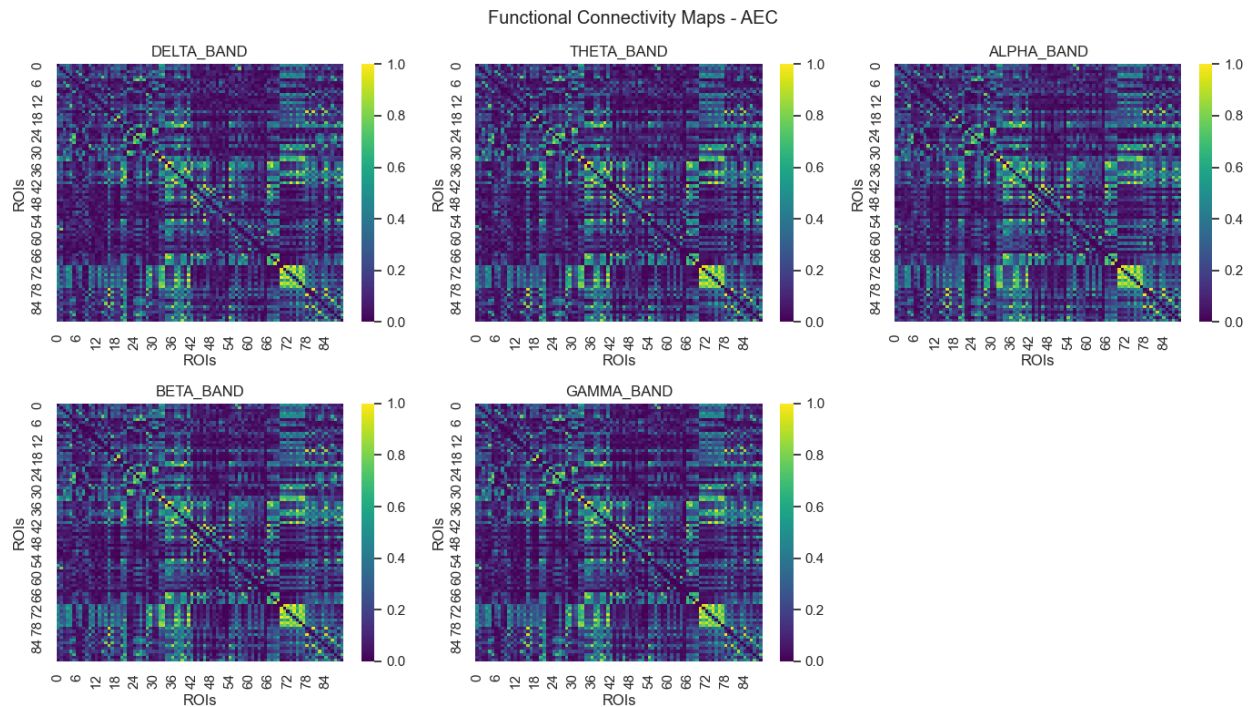

Figure 3.3.1. *The adjacency matrices of each frequency band / rhyme, using IPLV as FC estimator.*
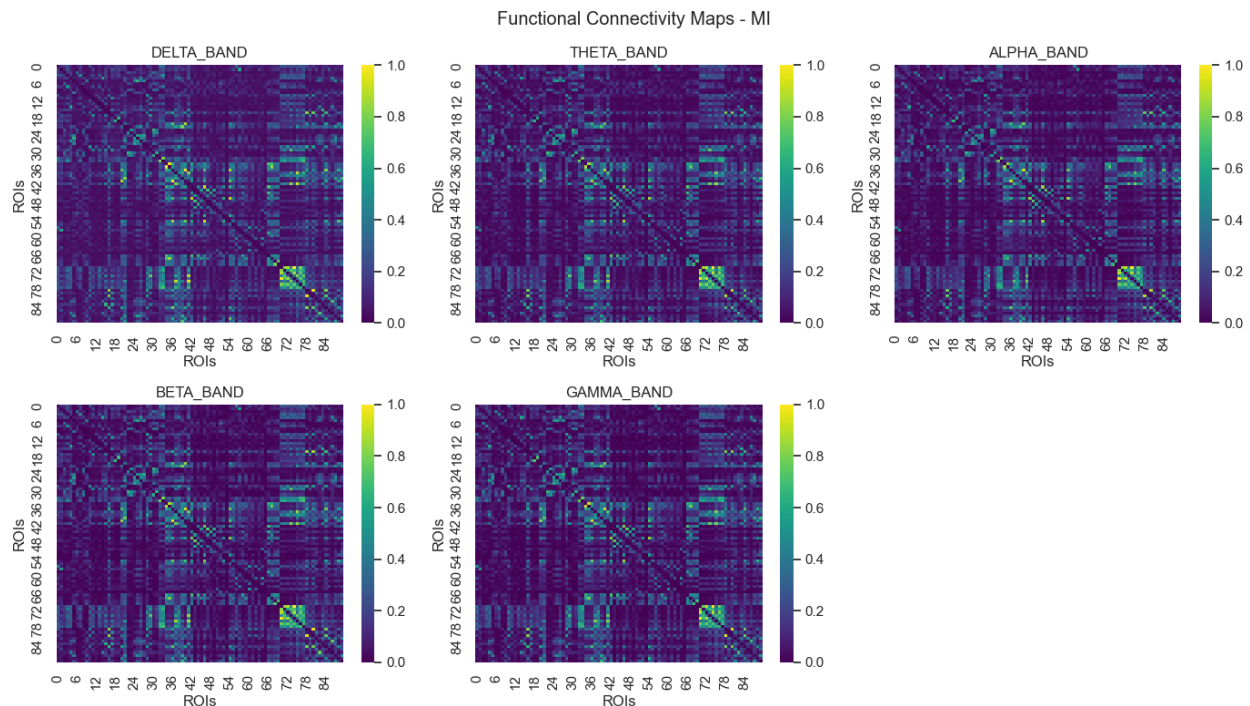

Figure 3.3.2. *The adjacency matrices of each frequency band / rhyme, using MI as FC estimator.*
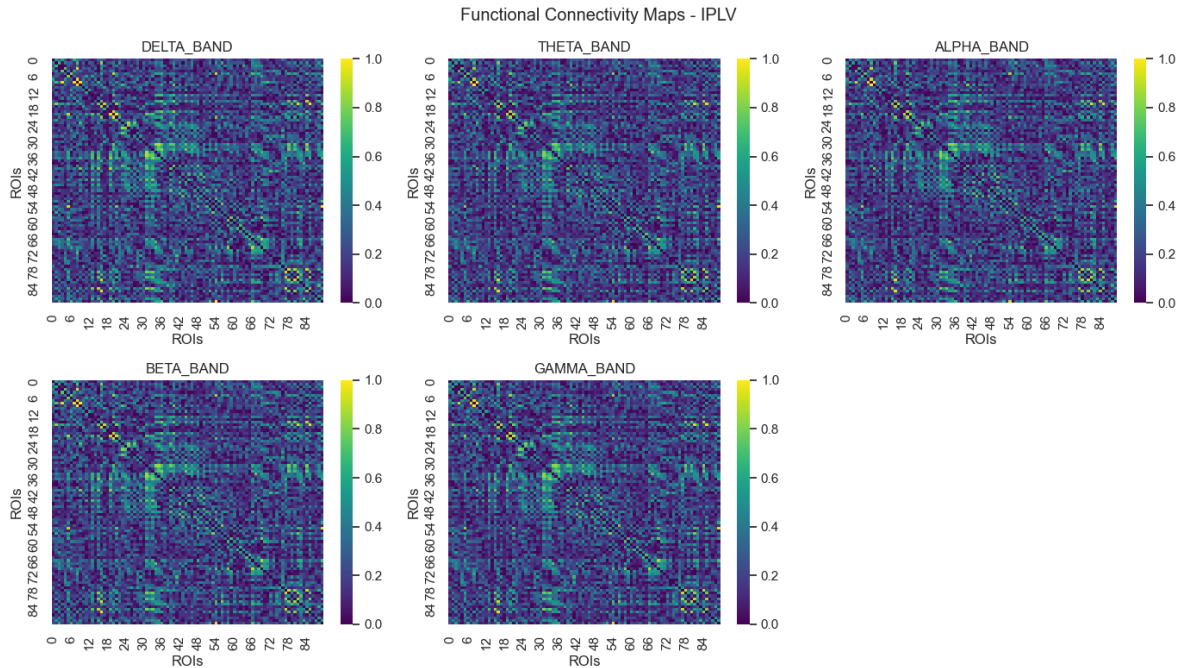
Figure 3.3.3. *The adjacency matrices of each frequency band / rhyme, using AEC as FC estimator.*

3.3 Edge Filtering

It is easy to assume that in this way links might get created that are spurious and are result of noise in brain signals. To overcome this problem, we enforced an edge filtering technique called Orthogonal Minimum Spanning Trees.

Orthogonal Minimum Spanning Trees (OMSTs) are an extension of the Minimum Spanning Tree (MST) approach, designed to offer a more comprehensive sampling of brain networks. While MSTs provide an unbiased method for obtaining reliable network metrics (Tewarie et al., 2014), they can be too sparse for large brain networks, potentially failing to capture the true topology and reducing discriminative power between groups (Dimitriadis et al., 2015; Antonakakis et al., 2016; Supekar et al., 2008; Brier et al., 2013; Khazaeea et al., 2017).

OMSTs address this limitation by constructing multiple MSTs that are orthogonal to each other, meaning they share no common edges. The process starts with an initial MST that connects all N nodes using $N-1$ edges. These edges are then set to zero, and a second MST is constructed that is orthogonal to the first. This process is repeated, each time creating a new MST that is orthogonal to all previous MSTs. In general, an m-MST will be orthogonal to the ($m-1$) previous MSTs and will have exactly $m \times (N-1)$ edges (Song et al., 2015).
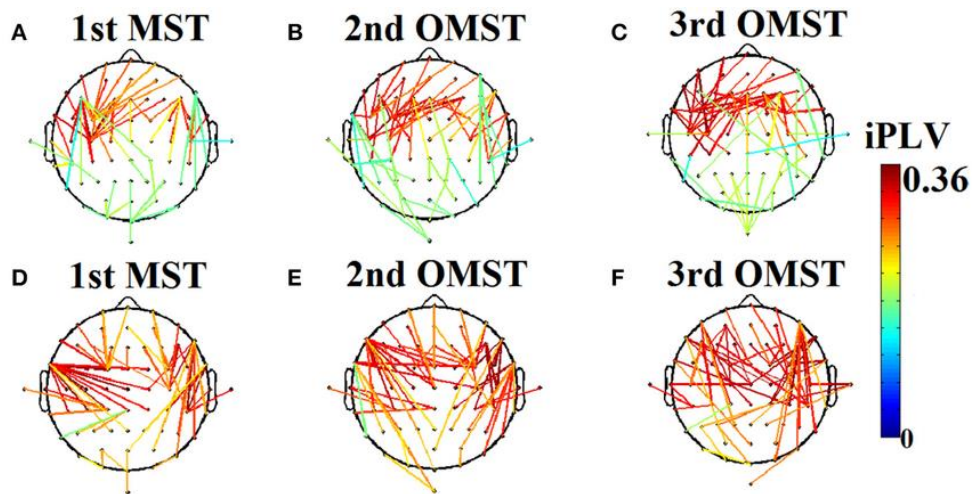
Figure 3.4. An application of Orthogonal Minimal Spanning Tree (OMSTs) applied to a static functional connectivity graph (FCG) from δ frequency bands during eyes-open condition (A–C) and eyes-closed condition (D–F) from https://www.researchgate.net/figure/An-app.

The computational time for this method is $O(m \times (N + E) \times \log V)$. OMSTs maintain the advantages of MSTs, such as connecting the entire network at a minimal cost without introducing cycles, while providing a richer, more nuanced representation of the network's topology. The implementation that was used in this research was like the one that Dimitriadis used in his publication (Dimitriadis, Salis, Tarnanas and Linden, 2017). The edge filtering was enforced after the creation of the brain networks, to eliminate as less important information as possible.

3.4 Network Topologies

Following the data preprocessing, we employed the adjacency matrices, also known as functional connectivity maps, to build the specific brain network topologies we aimed to investigate. These include the **Single Layer Network**, the **Multiplex Network**, and the **Full Multilayer Network**. In the subsequent sections, we will delve into the intricacies of how each of these networks is constructed and discuss their respective characteristics.

3.4.1 Single Layer Network

A Single Layer Network serves as a streamlined depiction of the brain's functional interactions, condensing the network into a single layer that captures statistical dependencies or temporal correlations among various brain regions. In this framework, nodes symbolize distinct Regions of Interest (ROIs), while edges represent the functional connections between these regions. In our study, these connections were quantified using iPLV, MI, and AEC. For instance, one Functional Connectivity (FC) map from Figure 2 constitutes a Single Layer Network, illustrating the functional connections occurring within a specific frequency band.

To maximize the utility of the available information, we chose to either aggregate or average across all frequency bands and estimators. This results in a unified network that offers a comprehensive, albeit less detailed, perspective on brain connectivity (Bullmore & Sporns, 2009; Rubinov & Sporns, 2010). In **Figure 3.5**, you can observe the resulted Single Layer Networks using our FC estimators. One way to achieve the aggregation of single-layer networks is by taking the average of the FC maps across each frequency band, thereby retaining the most crucial information. If the objective were to scrutinize the characteristics of individual frequency bands or identify the most influential one, aggregation would not be the appropriate approach, as it would compromise the integrity of the specific information within each band.
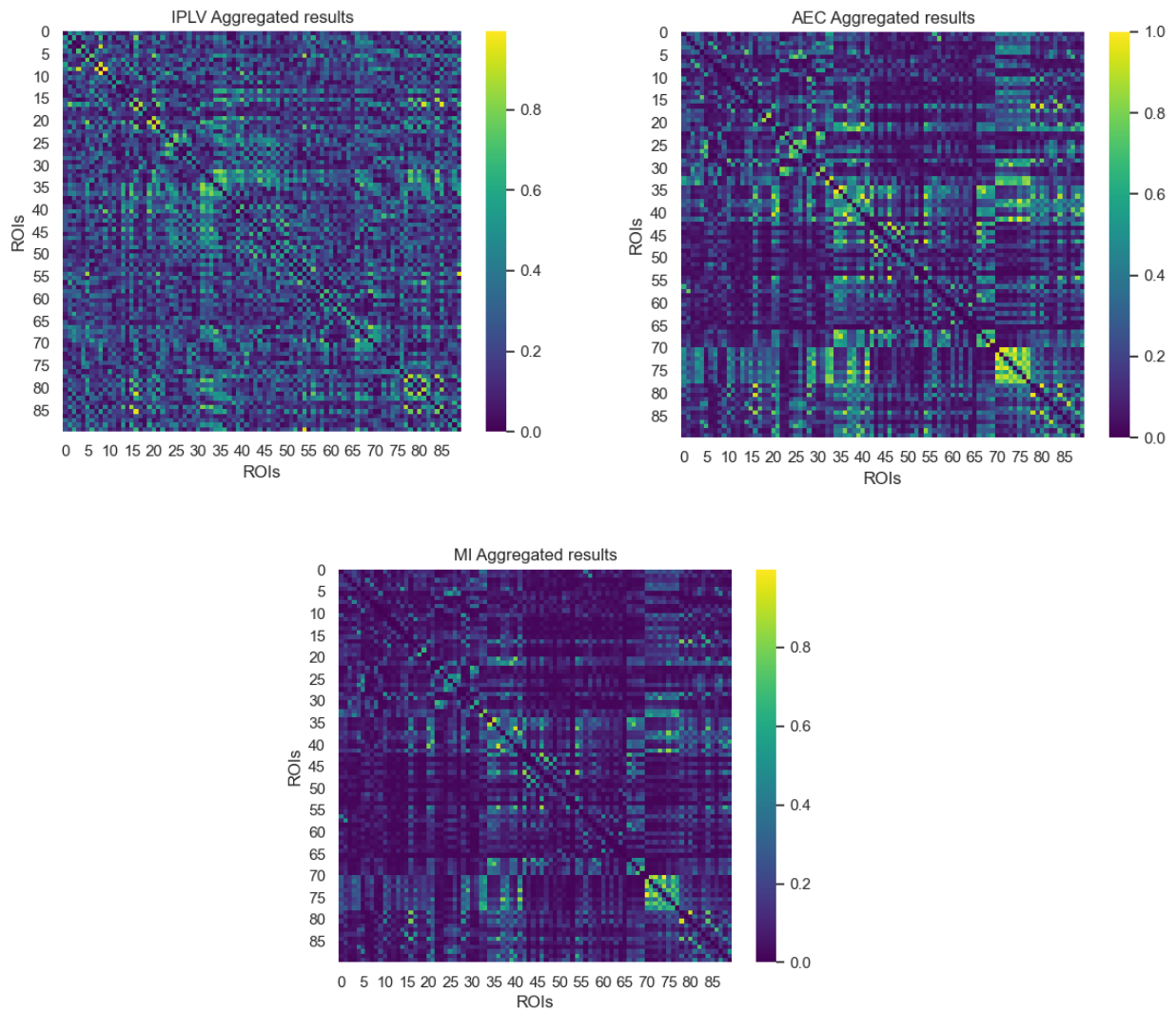
Figure 3.5. The aggregated Single Layer Networks using IPLV (left) and AEC (right) and MI (middle).

Upon implementing edge filtering via the Orthogonal Minimum Spanning Tree (OMST), the resulting adjacency matrices contain fewer details but retain the most robust connections among the signals. The heatmaps above display these filtered adjacency matrices for the aggregated single-layer representation, employing the chosen FC estimators. When compared to the matrices shown in **Figure 3.6**, it's evident that numerous previously calculated connections have been reduced to non-connections. This is because the OMST filtering method focuses on preserving the strongest links between the filtered signals, a process that is iteratively repeated (in this case, 15 times).
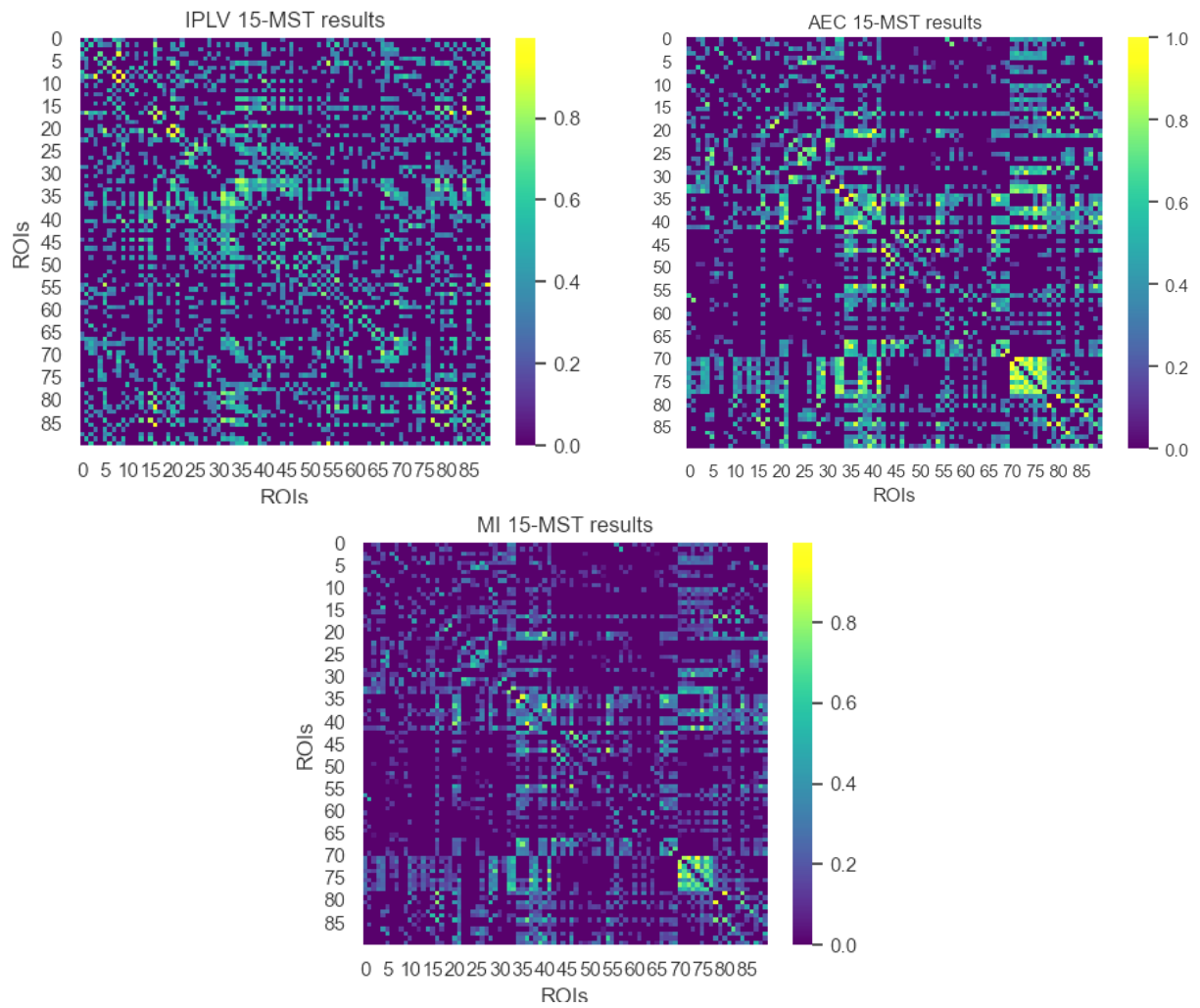
Figure 3.6. The aggregated Single Layer Networks using IPLV (left), MI (middle) and AEC (right) after the edge filtering through OMST.

3.4.2 Beyond the Single Layer: Multi-level Networks

Networks and complex systems are seldom isolated; they interact with other networks across various spatial and temporal scales. A case in point is transportation networks, where multiple layers of human mobility—from subway systems to airports and traditional roadways—can coexist in the same spatial framework.

Mathematical Representation. The concept of multilayer networks has gained traction relatively recently, with De Domenico et al. (2013) pioneering its mathematical formulation. Let $G = \{G_1, G_2, …, G_m\}$ represent the multiplex network, where G_i is the graph corresponding to the ith frequency band. Each graph $G_i = (V, E_i)$ consists of a set of vertices V (the ROIs) and a set of edges E_i representing functional connections at that frequency. The adjacency matrix A_i for each layer G_i can be defined as:

$$A_i = \left\{a_{ij}^{(i)}\right\}, \forall\, i, j\, \in 1, …, N$$

where $a_{ij}^{(i)}$ is the connectivity coefficient between node i and node j in the ith layer, often calculated using metrics like iPLV, MI, or AEC. In order for us to analyze the multilayer networks, we use a different representation, called supra-adjacency matrix.

In the realm of neuroscience, the use of multilayer networks is particularly promising due to the diverse types of brain connectivity networks available for study. A Multilayer Brain network captures the functional connectivity of the brain across different frequency bands. In this framework, each layer represents the brain's functional network at a specific frequency band (e.g., delta, theta, alpha, beta, gamma), and the same set of nodes (brain regions or ROIs) exists across all layers. Researchers commonly examine the synchronization of brain regions across different frequency bands, resulting in distinct functional networks. These networks can then be integrated into a multilayer framework, often referred to as frequency-based decomposition (Brookes et al. 2016; Buldú and Porter 2017; De Domenico, Sasai, and Arenas 2016).

Supra-adjacency Matrix. In the context of multilayer networks, a supra-adjacency matrix is a mathematical construct that encapsulates both intra-layer and inter-layer connections within a single matrix. This matrix serves as a comprehensive representation of a multilayer network, allowing for the analysis of complex systems that have multiple types of relationships or interactions across different layers (De Domenico et al., 2013). The supra-adjacency matrix S is a block matrix where each block S_{ij} represents the connections between nodes in layer i and layer j. If $i = j$, S_{ij} is the adjacency matrix of the ith layer. If $i \neq j$, S_{ij} contains the inter-layer edges between nodes in layer i and layer j. For a multilayer network with N nodes and M layers, the supra-adjacency matrix S is of size $N \times M$ by $N \times M$. To construct such data structure, we implement the following:

- **Intra-layer Edges**: The diagonal blocks of S are filled with the adjacency matrices of each layer.

- **Inter-layer Edges**: The off-diagonal blocks are filled based on the inter-layer connections between the same node across different layers. By using the supra-adjacency matrix, one can apply traditional graph-theoretical methods to multilayer networks, thereby extending the applicability of such methods to more complex systems.

MULTIPLEX NETWORK   SUPRA-ADJACENCY MATRIX
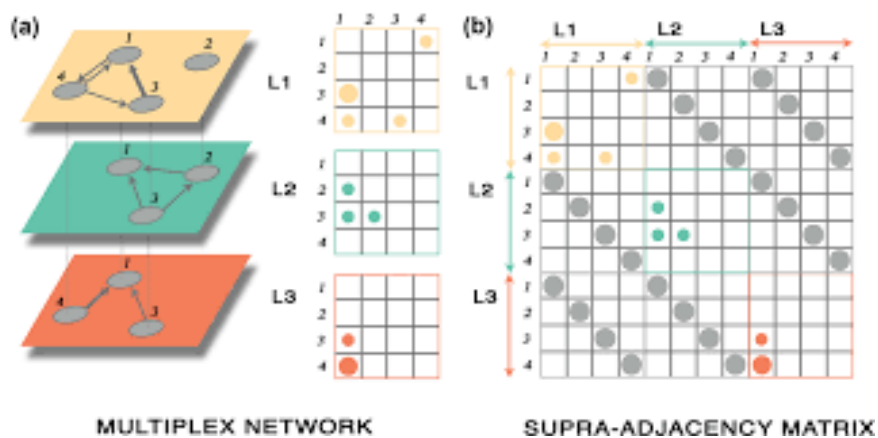
*Figure 3.7. (a) A multilayer network consists of different networks encoded by layers, each one represented by a (possibly directed and weighted) adjacency matrix. (b) Common representation of multilayer networks generally known as supra-adjacency matrix from https://www.semanticscholar.org/paper/Multilayer-modeling-and-analysis-of-human-brain-Domenico/d9a584cac9f9958271edc6deba23f11a21804fb0.*

Multiplex Network. A Multiplex Network is a specific type of multilayer network where each layer contains the same set of nodes, but the connections (edges) between the nodes can differ across layers. In the context of brain networks, each layer could represent functional connectivity at a different frequency band, and the nodes represent Regions of Interest (ROIs) in the brain. For illustrative purposes, **Figure 3.8.1, Figure 3.8.2** and **Figure 3.8.3** present visual representations of multiplex networks, providing insights into its structural complexity. The diagonal blocks display the adjacency matrices corresponding to each frequency band. Off-diagonal elements retain only the diagonal entries from each intra-layer adjacency matrix, indicating that nodes are connected to their corresponding nodes across different layers. Notably, the supra-adjacency matrix is a symmetric one.
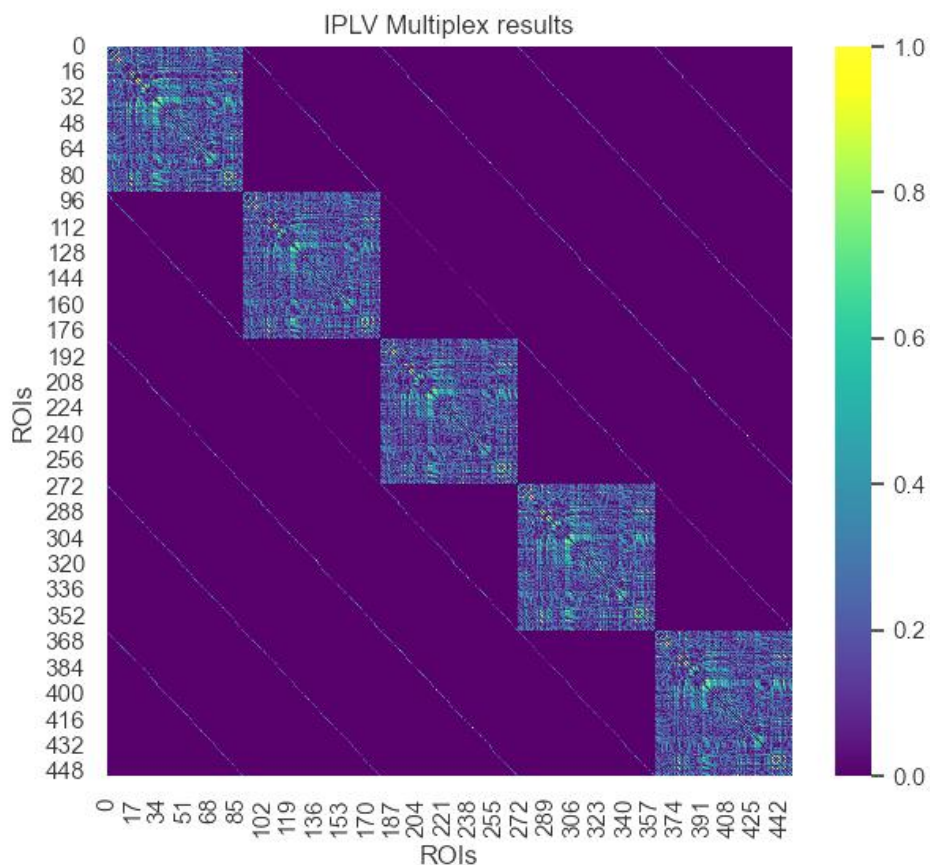
Figure 3.8.1. *The multiplex representation of brain FC networks, using IPLV as FC estimator.*
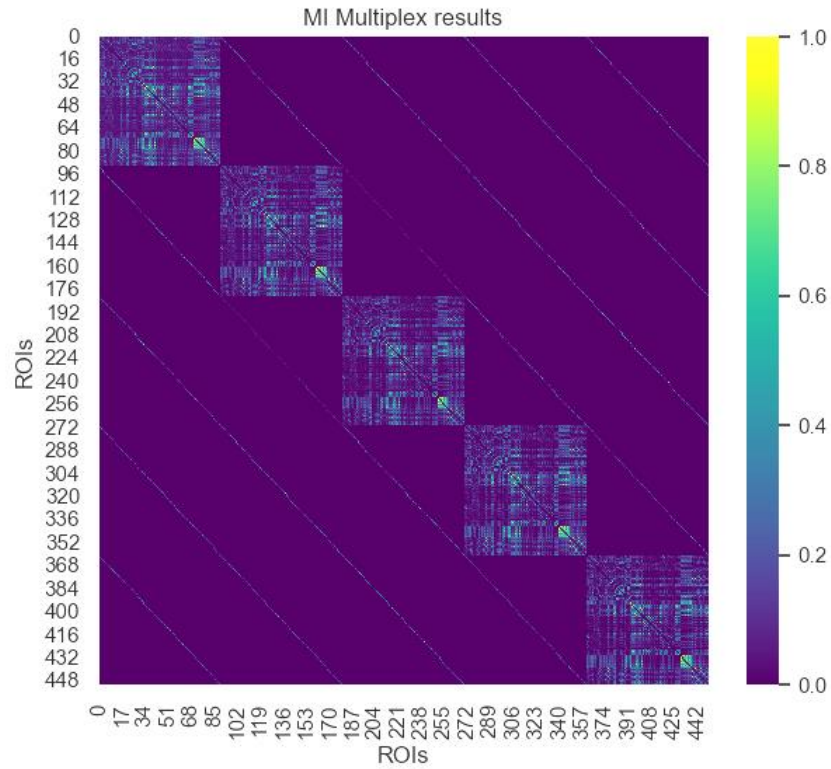
Figure 3.8.2. *The multiplex representation of brain FC networks, using MI as FC estimator.*
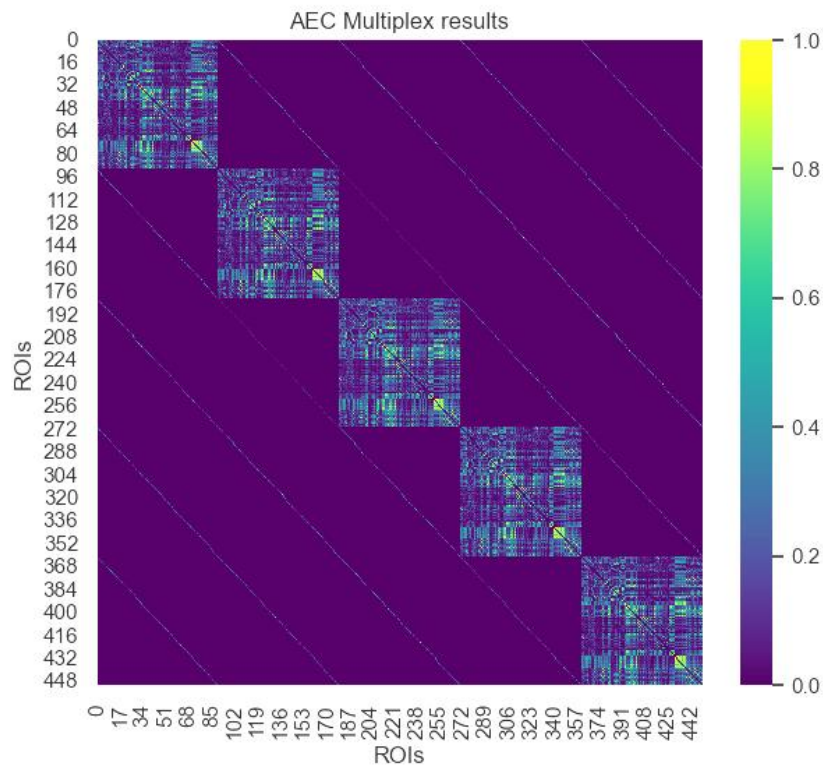
Figure 3.8.3. *The multiplex representation of brain FC networks, using AEC as FC estimator.*

Additionally, **Figure 3.9.1**, **Figure 3.9.2**, and **Figure 3.9.3** showcases the edge-filtered matrix is depicted, offering a refined view of the networks' connections. When compared to the matrices in Figure 3.6, it becomes evident that a significant number of previously established connections have been reduced to non-connections. The application of the OMST filtering method focuses on retaining only the strongest links between the filtered signals. The procedure is iteratively repeated, in this instance, 75 times. Importantly, even after this filtering process, many inter-layer connections remain intact, suggesting a high level of interaction between different layers.
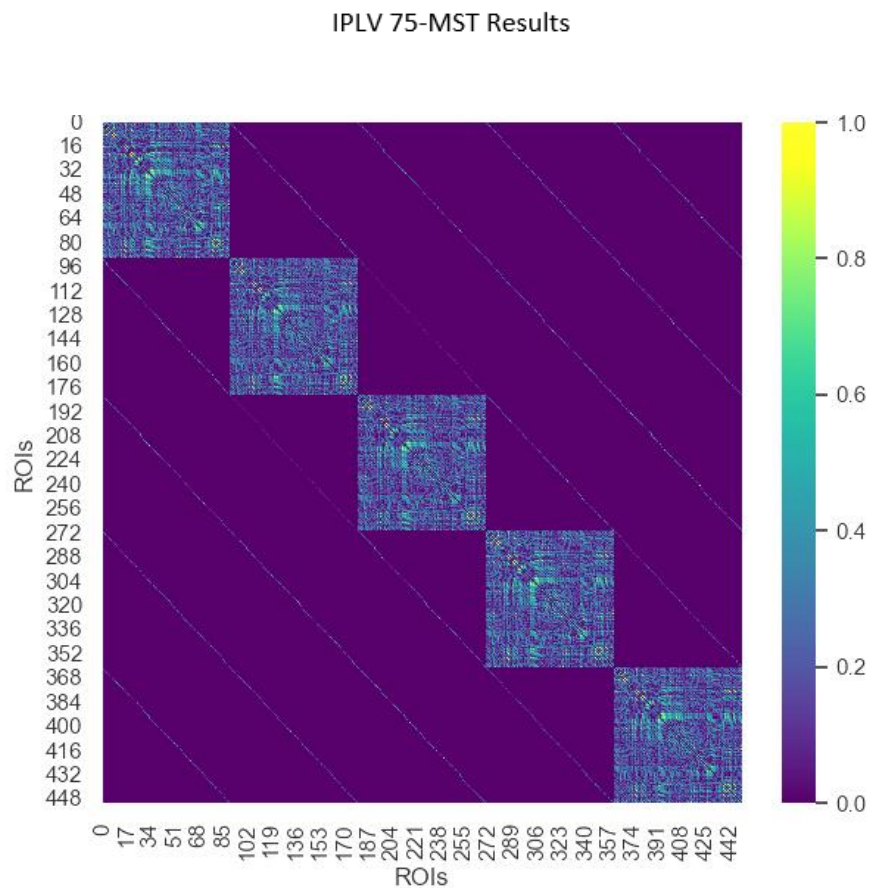
Figure 3.9.1. The Multiplex Brain Networks using IPLV, after applying edge filtering through OMST.
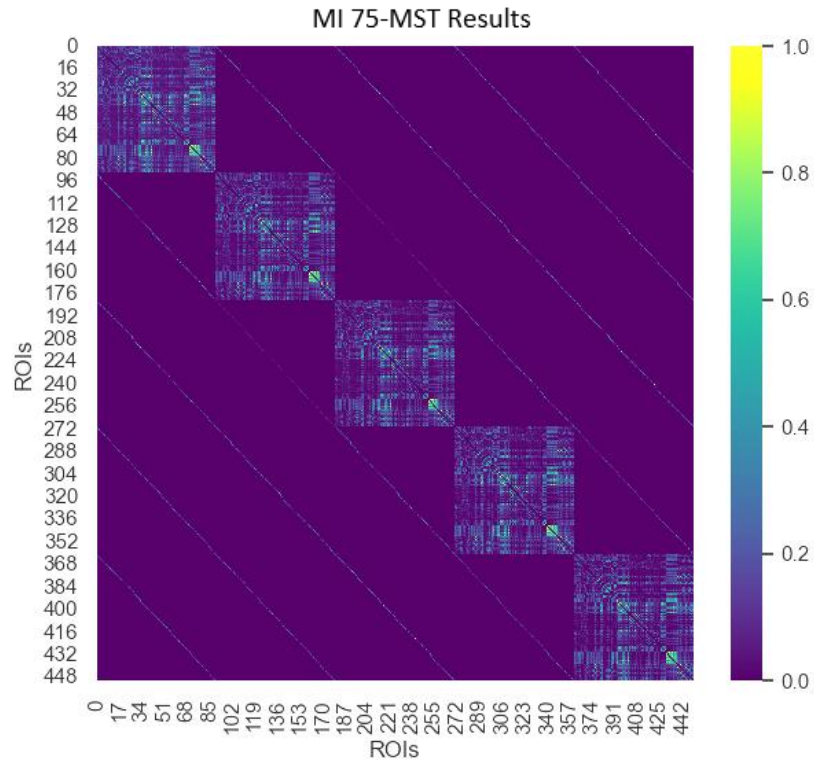
Figure 3.9.2. *The Multiplex Brain Networks using MI, after applying edge filtering through OMST.*
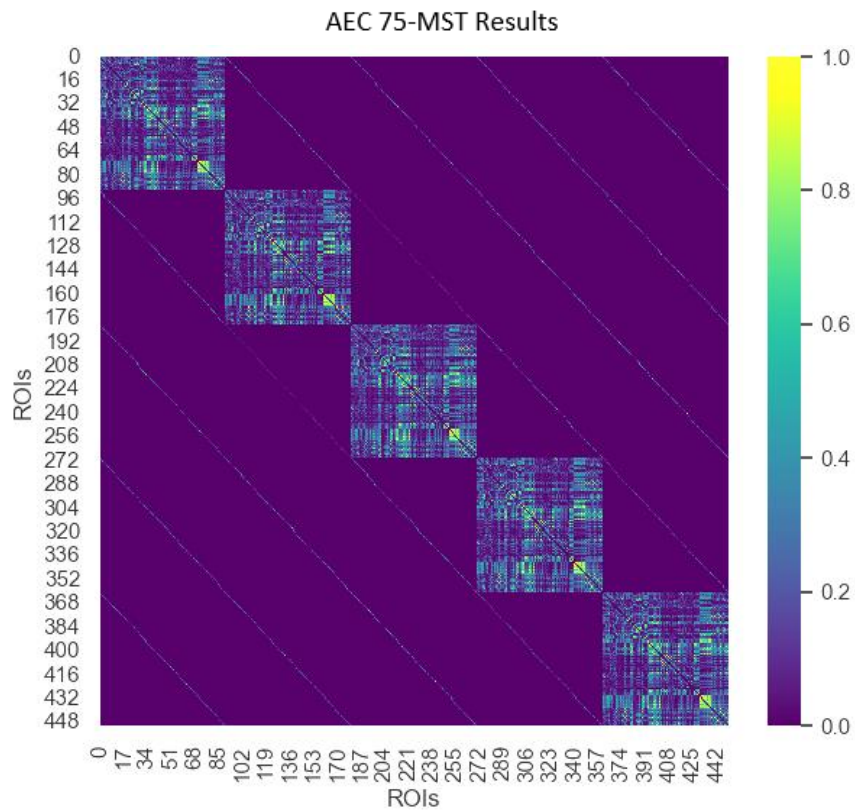
Figure 3.9.3. *The Multiplex Brain Networks using AEC, after applying edge filtering through OMST.*

Full Multilayer Network. A full multilayer network is an advanced structure that allows for the most general form of multilayered interactions among nodes. Unlike simpler forms like multiplex networks, a full multilayer network can accommodate different types of nodes and edges, multiple kinds of layers, and complex inter-layer connections. Each layer in a full multilayer network can represent a different type of relationship, interaction, or attribute, and nodes from one layer can be connected to nodes in the same or different layers.
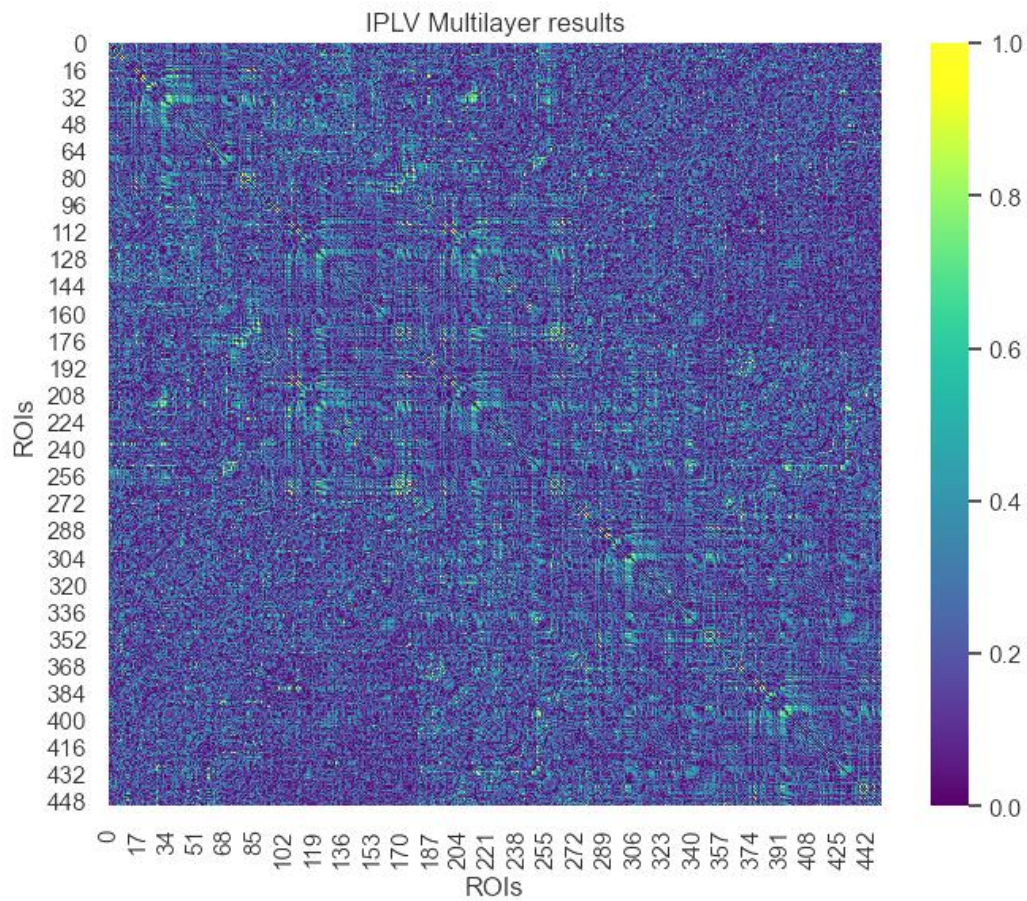
Figure 3.10.1 *The Full Multilayer Networks utilizing IPLV.*
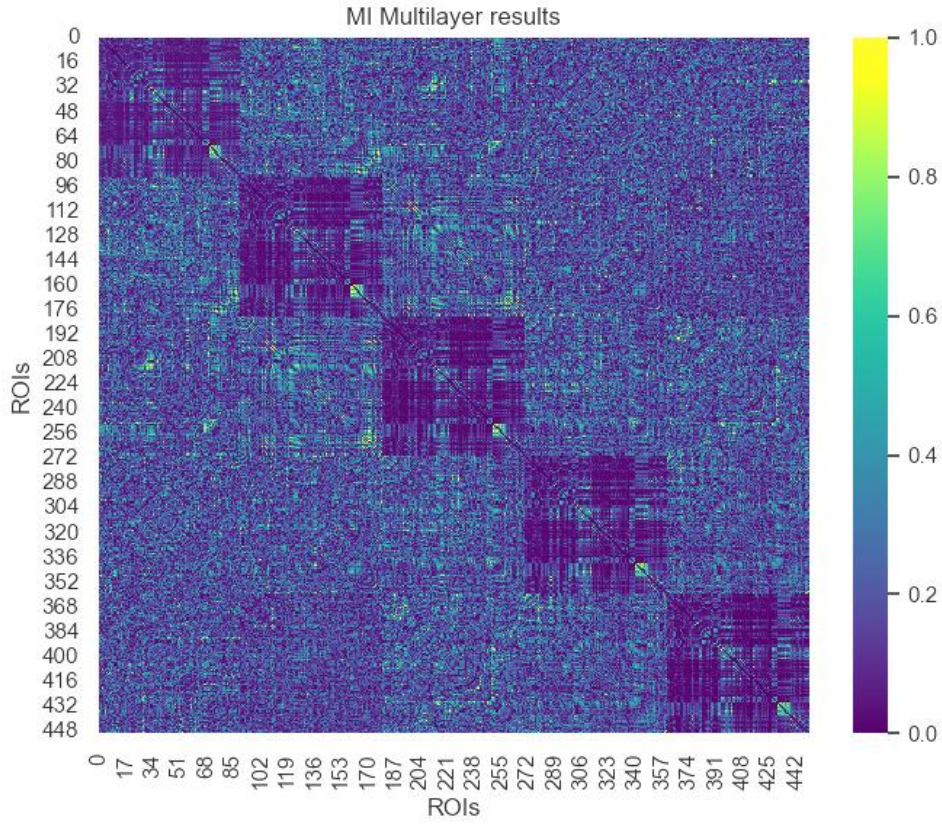
Figure 3.10.2 *The Full Multilayer Networks utilizing MI.*
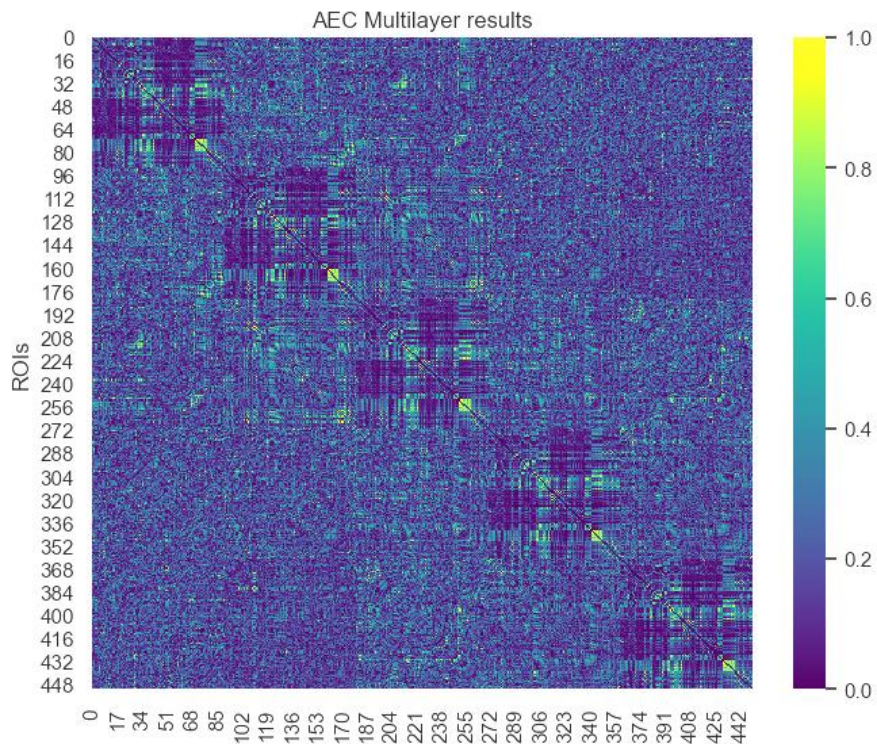
Figure 3.10.3 *The Full Multilayer Networks utilizing AEC.*

Above in **Figure 3.10.1**, **Figure 3.10.2**, and **Figure 3.10.3**, the full multilayer representation of our network is displayed. The differences between the full multilayer representation and the multiplex representation are quite clear. Proceeding, when employing the MI estimator, it becomes evident that inter-layer connections are more robust than intra-layer ones. A similar trend is noted with the AEC estimator, albeit to a lesser extent. This suggests that brain ROIs are more influenced by variations across different frequency bands than within the same band. Additionally, in each matrix, the upper right and lower left regions (owing to symmetry) appear darker than the rest. This indicates that connections between lower frequency bands (δ-θ) and higher frequency bands (β-γ) are relatively weaker.
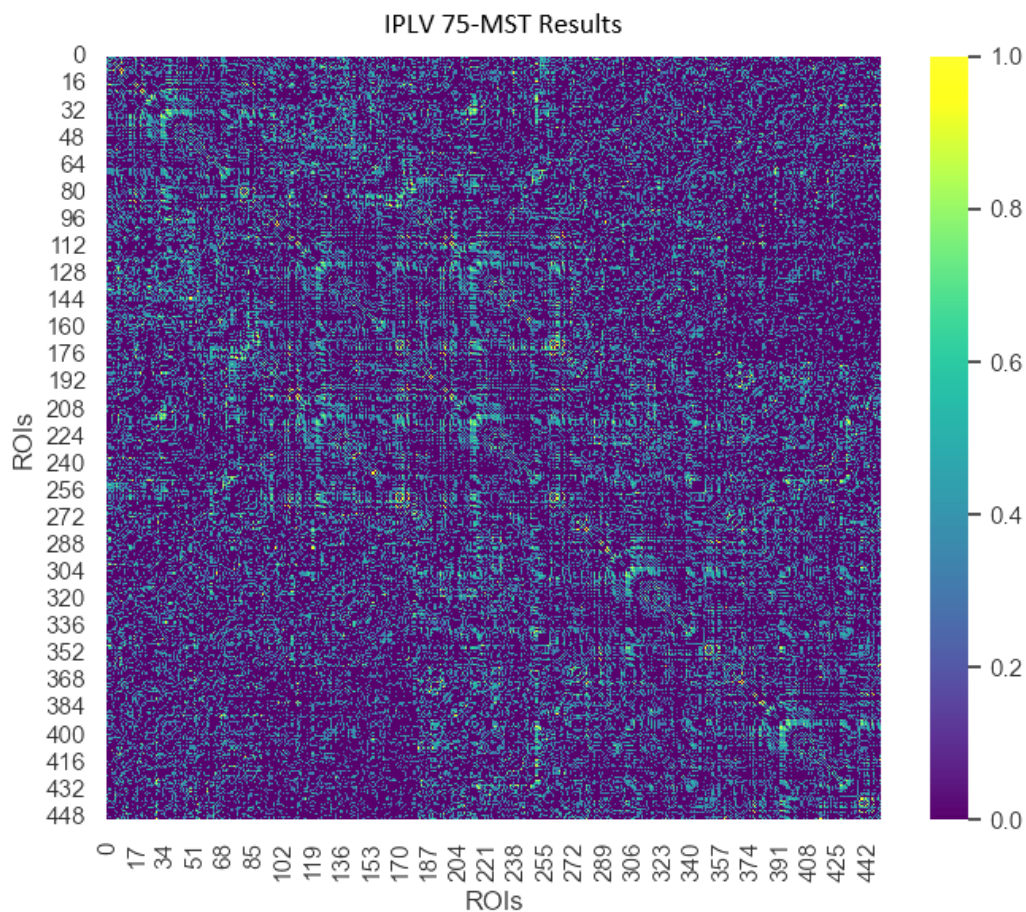

Figure 3.11.1. *The Full Multilayer Brain Networks using IPLV, after applying edge filtering through OMST.*
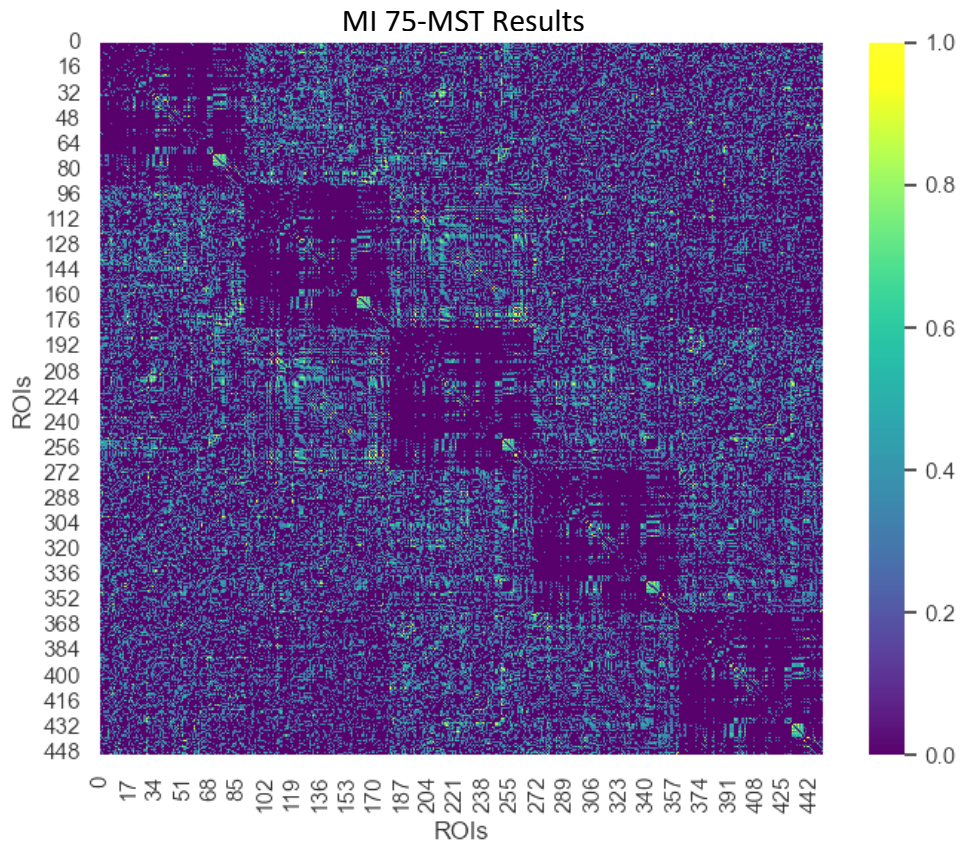
Figure 3.11.2. *The Full Multilayer Brain Networks using MI, after applying edge filtering through OMST.*
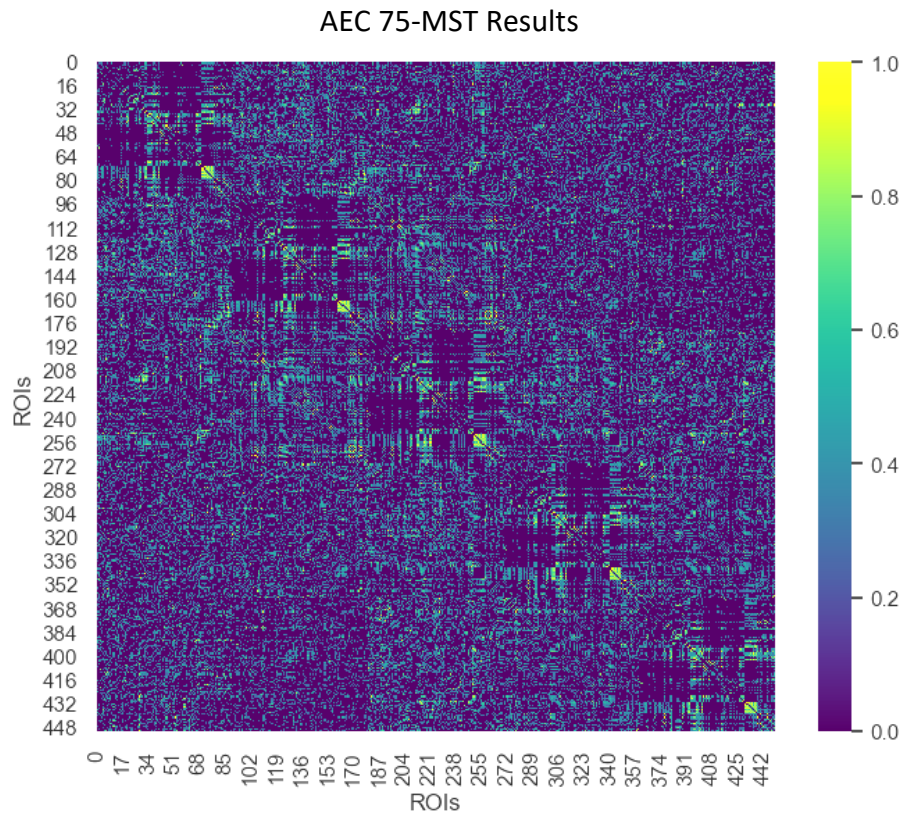

Figure 3.11.3. *The Full Multilayer Brain Networks using AEC, after applying edge filtering through OMST.*

The depiction of the same Full Multilayer Networks utilizing various FC estimators but with edge filtering applied agrees with the results observed on the previous figure. Furthermore, it can be observed that the strongest connections are along the diagonal blocks, though less in quantity.

3.5 Brain as a Graph

The human brain, often considered the most complex organ, can be represented as a network or graph to simplify the understanding of its intricate structure and functionalities. This graphical representation is not merely an academic exercise but serves as a foundational framework for various applications, including the study of neurological disorders, cognitive processes, and even machine learning algorithms for brain-computer interfaces. The construction of a brain graph from an adjacency matrix is a critical step in this direction.

3.5.1 Brain Visualization

In the previous section, we defined what an adjacency matrix is. We can use this data representation to construct a graphical model using software tools or custom algorithms. The elements of the matrix indicate whether pairs of vertices are adjacent or not in the graph. In the context of a brain graph, each vertex or node represents a Region of Interest (ROI) in the brain, and the edges between them signify functional connections.

Before, we defined what an adjacency matrix is. We can use this data representation to construct a graphical model using software tools or custom algorithms. The elements of the matrix indicate whether pairs of vertices are adjacent or not in the graph. In the context of a brain graph, each vertex or node represents a Region of Interest (ROI) in the brain, and the edges between them signify functional connections.

Leveraging the capabilities of the Python's **matplotlib** library, we successfully visualized the brain network in a graphical format, as depicted in **Figure 3.12**. In this representation, each node signifies a Region of Interest (ROI), clearly labeled adjacent to it. These nodes are interconnected by edges, the colors of which denote the varying strengths of connections as determined by the Functional Connectivity (FC) estimator.
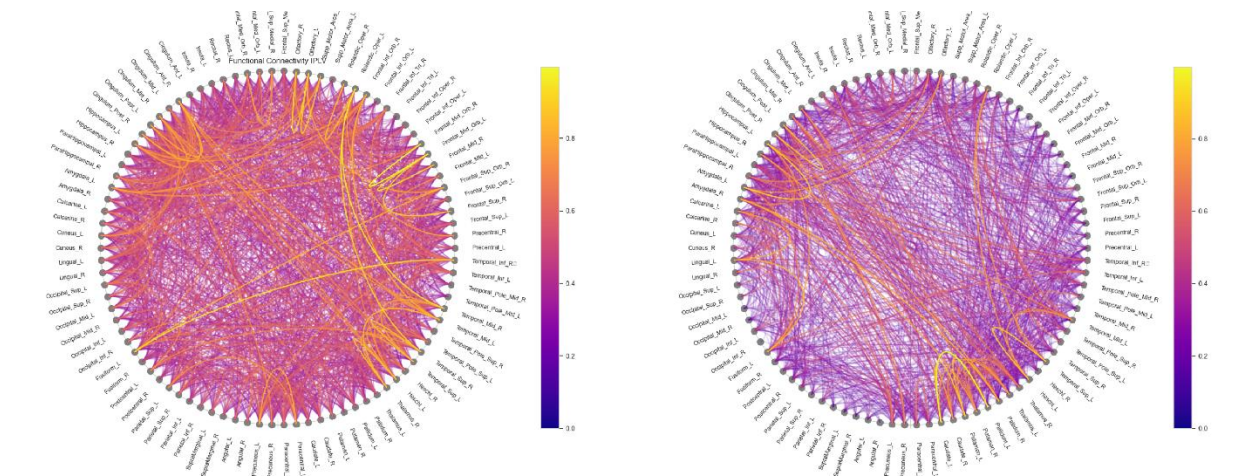
Figure 3.12. *Chord Plots of Brain Networks utilizing IPLV (top-left), MI (top-right), AEC (bottom).*

Upon analysis, the graph elucidates the density and distribution of connections in each case. Notably, the IPLV appears to facilitate a more balanced distribution of connection strengths compared to MI and AEC. While MI exhibits a handful of potent connections, AEC demonstrates a plethora of strong connections. Furthermore, it is evident that there is a significant correlation between one ROI in one hemisphere and its counterpart in the opposite hemisphere. Interestingly, the graph also unveils

connections between ROIs that are geographically distant from each other, hinting at the complex and non-linear nature of brain networks.

However, this graphical representation has its limitations, particularly for individuals unfamiliar with the anatomical locations of the ROIs within the brain. To mitigate this, we utilized another visualization tool, **visbrain**, which offers a more intuitive platform for comprehending our findings, especially in terms of spatial relationships and connectivity patterns within the brain (Combrisson E et al., 2019).

Figure 3.13. *Depiction of brain with connections from AEC (visbrain). Here displayed side, top, and front view.*
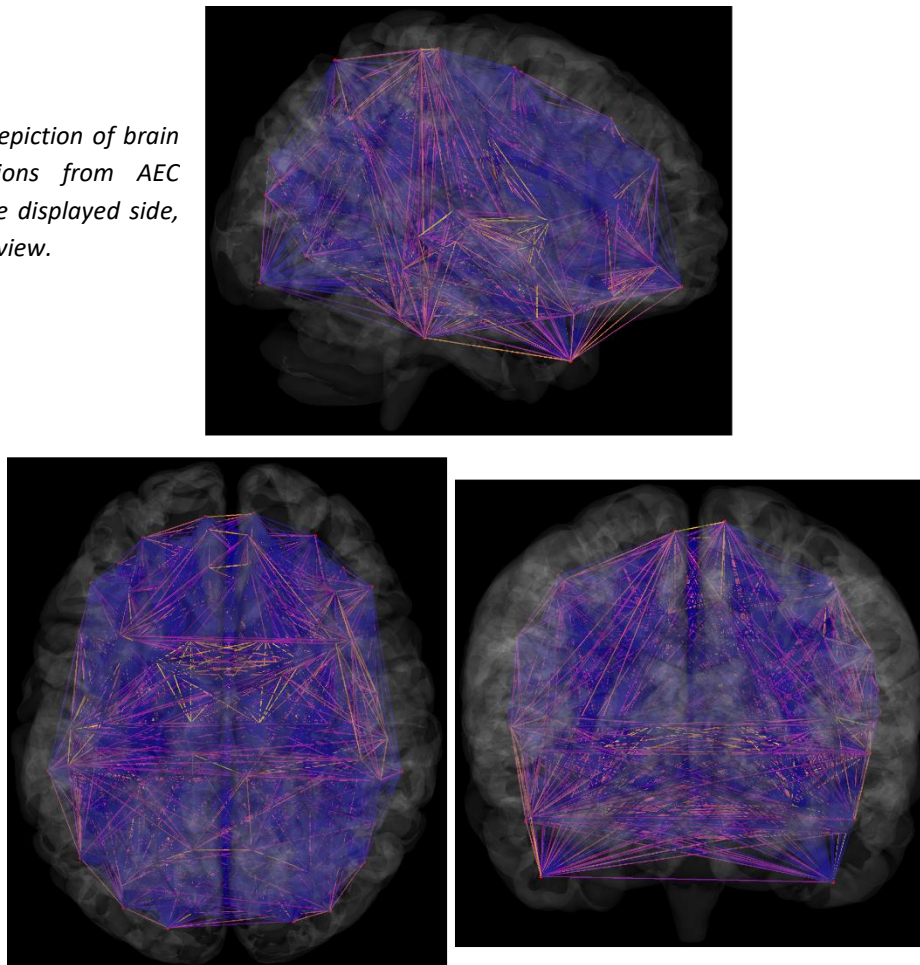
The results from the previous analysis are now validated. It is obvious that indeed most connections are made among close nodes. Notable in the case of AEC is that the strongest connections are noticed in the frontal lobe, the region responsible for planning, concentration, and speech.

3.5.2 Graph Features

Constructing a brain graph serves as a strategic approach to streamline the complex neurological data into a more digestible and interpretable format. Leveraging graph theory, we can employ a set of straightforward yet potent tools to dissect various facets of the brain network, thereby facilitating a clearer understanding of brain functionalities and potentially aiding in the identification of different disorders. This graphical representation not only organizes the intricate data in a more structured manner but also lays the groundwork for implementing diverse analytical methods that can yield deep insights into the functioning of the human mind. In this section, we will focus on analyzing select pivotal features of the graph, which are instrumental in unraveling the complex dynamics of brain networks.

Nodal Strength (NS) is computed as the sum of the weights of the connections (edges) linked to a specific node. In the context of an adjacency matrix, it can be calculated by summing the values in a row corresponding to that node. Mathematically, the node strength (NS_i) for node *i* is given by:

$$NS_i = \sum_{j=1}^{N} A_{ij}$$

where NS_i is the node strength of node *i, N* the number of nodes and A_{ij} the element of the adjacency matrix representing the connection weight between nodes *i* and *j.* This calculation is performed for each node in the network, creating a feature vector *NS* = (NS_1, NS_2, ..., NS_N) that encapsulates the node strengths across the network (Klepl et al., 2022). In a multiplex network, node strength can be calculated separately for each layer and then combined to get a comprehensive view. The node strength in a multilayer network would be the sum of the weights of connections a node has in all layers, considering both intra-layer and inter-layer connections.

Characteristic Path Length (CPL). The characteristic path length in a brain network is a significant metric in understanding the functional connectivity and organization of the brain. It is defined as the average shortest path length between all pairs of nodes in the network, offering insights into the efficiency of information transfer in the network. The feature is calculated using the following formula:

$$CLP = \frac{1}{N\,(N-1)} \sum_{i \neq j} d(i,j)$$

where *N* is the number of nodes in the network and *d(i, j)* is the shortest path length between node *i* and node *j*. The summation runs over all pairs of nodes, excluding self-loops (Fraschini et al., 2016; Guillon, 2018). The characteristic path length in a multilayer network would consider the shortest paths between nodes that might traverse through different layers. It would be a more complex calculation involving both intra-layer and inter-layer connections to find the most efficient path across the entire multilayer structure.

Global Efficiency (GE) is a metric that quantifies the efficiency of information transfer in a network. It is computed as the average of the inverse shortest path length between all pairs of nodes in the network. The mathematical representation of global efficiency is given by:

$$GE = \frac{1}{N\,(N-1)} \sum_{i \neq j} \frac{1}{d(i,j)}$$

where *N* is the number of nodes in the network, and *d(i, j)* is the shortest path length between nodes *i* and *j*. While the characteristic path length gives an average measure of the shortest distances, global efficiency considers the reciprocal of these distances, thus emphasizing the efficiency of information transfer (Pasquale et al., 2016; Guillon, 2018). Global efficiency in a multilayer network would consider the efficiency of information transfer across all layers. It would involve calculating the reciprocal of the harmonic mean of the shortest path lengths across layers, integrating the efficiencies of individual layers into a global metric.

Nodal Betweenness Centrality (NBC) is a measure that quantifies the influence of a node in a network, indicating how often a node acts as a bridge along the shortest path between two other nodes. It can be mathematically represented as:

$$NBC_i = \sum_{s \neq i \neq t} \frac{\sigma_{st}(i)}{\sigma_{st}}$$

where NBC_i is the betweenness centrality of node i, σ_{st} is the total number of shortest paths from node s to node t, and $\sigma_{st}(i)$ is the number of those paths that pass-through node i. In the context of brain networks, betweenness centrality can help identify regions of the brain that play a critical role in facilitating communication between other regions. High betweenness centrality values indicate nodes that are well-placed to influence the network's information flow, potentially serving as hubs in the network (Banks et al., 2016; Guillon, 2018). In a multilayer network, betweenness centrality would consider the nodes that act as bridges not only within a layer but also between different layers. It would quantify the influence of a node in facilitating communication between nodes in different layers, thus having a more global perspective.

Modularity (Q). In the context of brain networks, modularity refers to the extent to which the network can be segregated into densely connected groups of regions, or modules, with sparse connections between them. A high modularity indicates a greater degree of segregation, where connections are denser within modules and sparser between different modules. This metric can be used to predict individual responses to interventions such as cognitive training or physical exercise, with higher baseline modularity often associated with greater improvements in cognitive functions. Mathematically, the modularity Q of a network is given by:

$$Q = \frac{1}{2m} \sum_{ij} \left(A_{ij} - \frac{k_i k_j}{2m} \right) \delta(g_i, g_j)$$

where A_{ij} is the adjacency matrix representing the network, k_i and k_j are the degrees of nodes *i* and *j*,

m is the total number of edges in the network, g_i and g_j are the modules to which nodes *i* and *j* belong,

$\delta(g_i, g_j)$ is the Kronecker delta function, which equals 1 if $g_i = g_j$ and 0 otherwise. This metric can be

a valuable tool in understanding the functional organization of brain networks, particularly in the

context of rehabilitation and cognitive training interventions (Arnemann et al., 2015; Baniqued et al.,

2018; Guillon, 2018). Modularity in a multilayer network would consider the community structure across

layers. It would involve identifying modules that are consistent across layers, indicating a hierarchical

and multi-resolution community structure in the network.

Participation Coefficient (P). The participation coefficient in a brain network is a metric that

quantifies the extent to which a node (or brain region) connects to multiple modules or communities

within the network. It serves as an indicator of the node's role in facilitating integration between

different functional groups in the brain. A node with a high-participation coefficient acts as a connector

hub, linking different communities and thus playing a crucial role in the network's global integration

(Pedersen et al., 2017; Guillon, 2018). To calculate the participation coefficient (P) of a node i, the

following formula is used:

$$P_i = 1 - \sum_{s=1}^{N} \left(\frac{k_{is}}{k_i} \right)^2$$

Where:

- k_{is} is the number of links of node i to nodes in module s

- k_i is the total degree of node i (sum of all connections)

- N is the number of modules in the network

In a multilayer network, the participation coefficient would quantify the extent to which a node

connects to multiple communities across different layers. It would indicate nodes that have a significant

role in integrating information across different functional groups in the network.

Assortativity (r) in a brain network is a measure that indicates the preference of a node to connect with other nodes that have a similar degree of connections. In other words, it quantifies the correlation of the degrees of connected nodes within the network. A positive assortativity coefficient indicates that nodes tend to connect with others of similar degree, fostering a resilient and cohesive network structure. Conversely, a negative coefficient suggests a tendency for nodes to connect with others of dissimilar degree, which might indicate a hierarchical or centralized network structure (Bahrami et al., 2015). The assortativity coefficient (r) can be calculated using the following formula:

$$r = \frac{\sum_{ij}(k_i - \bar{k})(k_j - \bar{k})}{\sum_{ij}(k_i - \bar{k})^2}$$

Where k_i and k_j are the degrees of nodes i and j, respectively and $\bar{k}$ is the average degree of the nodes in the network. The sums run over all edges of the network. Assortativity in a multilayer network would consider the degree correlations across layers. It would involve calculating the tendency of nodes to connect with others of similar degree within and across layers, indicating the mixing patterns in the multilayer structure.

3.5.3 Signal Features

Apart from the graph features that are used to feed the Machine Learning Classifiers, we also need to extract meaningful features from the original signals to give as input to the GCN. So, a diverse array of signal features is employed, providing a comprehensive understanding of the underlying neurological processes. These features play a crucial role in characterizing the intricate dynamics within the brain and pave the way for subsequent analyses. In this section, we delve into several key signal features, shedding light on their significance in unraveling the complexities of brain activity.

Mean Value (μ): The mean value is a fundamental statistical feature that quantifies the central tendency of a signal. It is computed as the arithmetic average of the signal samples within a defined time window. Mathematically, the mean value (μ_i) for a signal i is given by:

$$\mu_i = \frac{1}{N} \sum_{j=1}^{N} x_{ij}$$

Where μ_i represents the mean value of signal i, N is the number of samples in the time window, and x_{ij} represents the j-th sample of signal i. The mean value provides valuable information about the signal's baseline and overall distribution, aiding in the characterization of signal stability and average activity levels.

Root Mean Square (RMS) Value: The RMS value serves as a fundamental feature, encapsulating the amplitude-related information of the signals. It is calculated by taking the square root of the mean of the squared values of the signal samples over a specific time window. Mathematically, the RMS value (RMS_i) for a signal i is defined as:

$$RMS_i = \sqrt{\frac{1}{N} \sum_{j=1}^{N} x_{ij}^2}$$

Here, RMS_i represents the RMS value of signal i, N denotes the number of samples in the time window, and x_{ij} represents the j-th sample of signal i. The RMS value provides valuable insights into the overall intensity of neural activity, aiding in the assessment of signal magnitude and variations over time.

Curve Length (CL): Curve length is a significant feature that measures the overall trajectory or path length of a signal in its waveform. It quantifies the extent to which a signal deviates from a straight line within a specified time window, providing insights into the signal's complexity and waveform irregularities. Mathematically, the curve length (CL_i) for a signal i is computed as:

$$CL_i = \sum_{j=2}^{N} \left| x_{ij} - x_{i(j-1)} \right|$$

Here, CL_i represents the curve length of signal i, N is the number of samples in the time window, and x_{ij} represents the j-th sample of signal i. Curve length analysis enables the characterization of signal intricacies, including oscillatory patterns, rapid changes, and variations in amplitude, making it a valuable feature for assessing signal complexity.

Zero Crossings (ZC): Zero crossings represent a fundamental feature in signal analysis, denoting the points in a signal where it changes polarity, crossing the zero-amplitude threshold. Counting the number of zero crossings within a signal provides insights into its frequency content and rapid changes. Mathematically, the zero crossings (ZC_i) for a signal i are calculated as:

$$ZC_i = \sum_{j=2}^{N} \begin{cases} 1, if\ x_{ij} \cdot x_{i(j-1)} < 0 \\ \quad 0, otherwise \end{cases}$$

Here, ZC_i represents the zero crossings of signal i, N is the number of samples in the signal, and x_{ij} represents the j-th sample of signal i. Zero crossings offer valuable insights into the temporal dynamics and frequency characteristics of the signal.

Intensity Weighted Mean Frequency (IWMF): The intensity-weighted mean frequency is a feature that provides information about the central frequency of a signal while considering the amplitude or intensity of each frequency component. It allows for a weighted assessment of the dominant frequency content in a signal. Mathematically, the intensity-weighted mean frequency ($IWMF_i$) for a signal i is calculated as:

$$IWMF_i = \frac{\sum_{k=1}^{K} f_k \cdot A_{ik}}{\sum_{k=1}^{K} A_{ik}}$$

Here, $IWMF_i$ represents the intensity-weighted mean frequency of signal i, K is the number of frequency components, f_k represents the frequency of the k-th component, and A_{ik} represents the

amplitude or intensity of the k-th component in signal i. This feature provides a weighted measure of the central frequency based on the relative importance of different frequency components.

Intensity Weighted Bandwidth (IWB): The intensity-weighted bandwidth is a feature that characterizes the spread or width of the frequency spectrum in a signal while considering the amplitude or intensity of each frequency component. It offers insights into the distribution of frequency components around the central frequency. Mathematically, the intensity-weighted bandwidth (IWB_i) for a signal i is calculated as:

$$IWB_i = \frac{\sum_{k=1}^{K} |f_k - IWMF_i| \cdot A_{ik}}{\sum_{k=1}^{K} A_{ik}}$$

Here, IWB_i represents the intensity-weighted bandwidth of signal i, K is the number of frequency components, f_k represents the frequency of the k-th component, $IWMF_i$ is the intensity-weighted mean frequency of signal i (calculated as described earlier), and A_{ik} represents the amplitude or intensity of the k-th component in signal i. This feature provides a weighted measure of the frequency spectrum's width based on the relative importance of different frequency components.

Spectral Entropy (SE): Spectral entropy is a feature that quantifies the randomness or complexity of the frequency distribution within a signal's spectrum. It assesses the degree of spectral diversity and can reveal the presence of distinct frequency components or irregularities. Mathematically, the spectral entropy (SE_i) for a signal i is calculated as:

$$SE_i = -\sum_{k=1}^{K} P_{ik} \cdot log_2(P_{ik})$$

Here, SE_i represents the spectral entropy of signal i, K is the number of frequency components, P_{ik} represents the normalized power or probability of the k-th component in signal i. Spectral entropy

provides insights into the signal's frequency complexity, with higher values indicating greater spectral diversity.

Absolute Area (AA): The absolute area is a feature that quantifies the total area under the signal's waveform, disregarding its polarity. It provides a measure of the overall magnitude or energy of the signal, regardless of its direction. Mathematically, the absolute area (AA_i) for a signal i is calculated as:

$$AA_i = \sum_{j=2}^{N} \left| x_{ij} - x_{i(j-1)} \right|$$

Here, AA_i represents the absolute area of signal i, N is the number of samples in the signal, and x_{ij} represents the j-th sample of signal i. Absolute area analysis captures the total magnitude of signal fluctuations, offering insights into its energy content.

Additional features, including Peak-to-peak voltage, cross-correlation, and various graph-theoretical measures, were evaluated but ultimately not included in the feature selection. The chosen features, as previously delineated, provide significant discriminative power in differentiating healthy controls from mTBI patients. The efficacy of these selected features is further evidenced by the boxplots presented below, which visually reinforce their distinction between the two groups. The robustness of these features is supported by their ability to capture essential patterns and differences in the brain's functional connectivity that are indicative of mTBI.
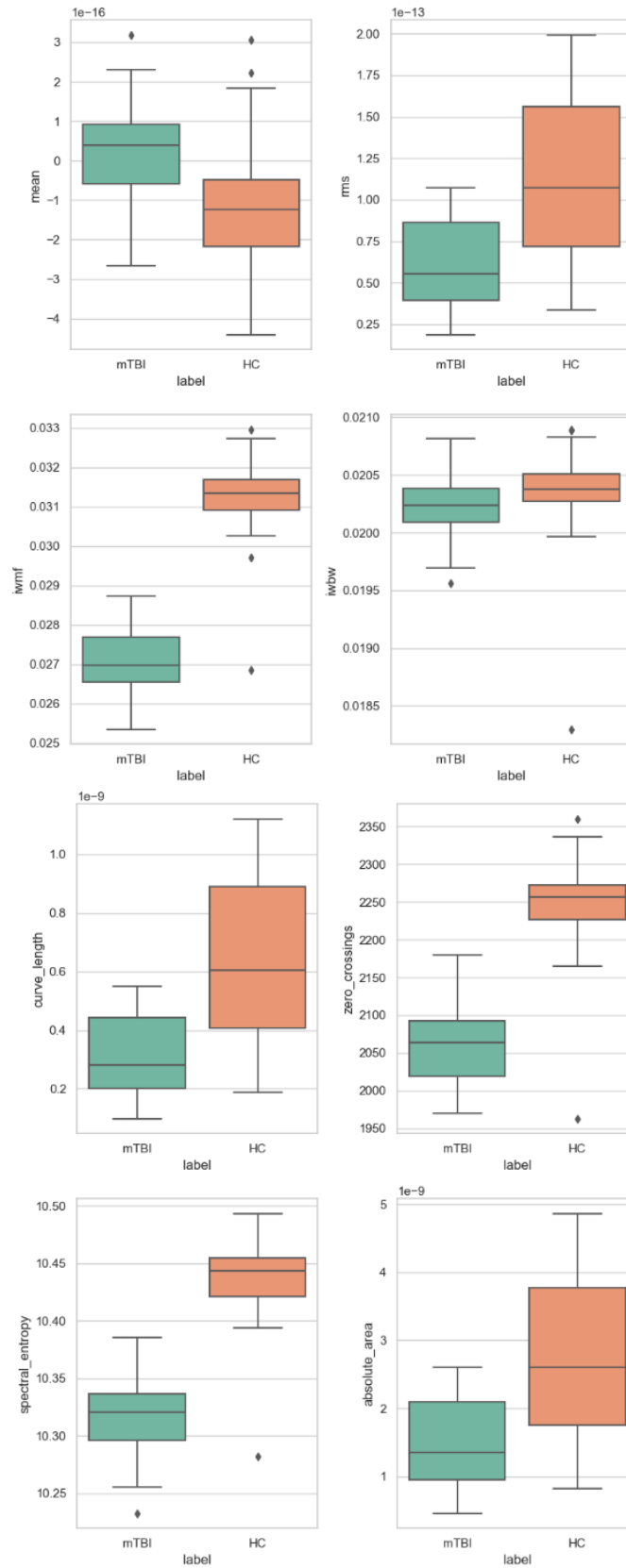
Figure 3.14 *Boxplots indicating the mean value and the deviation of each feature for HC and mTBI*

The subsequent chapter will delve into the classification of these brain graphs and matrices. Understanding the types and characteristics of different brain graphs is essential for their effective utilization in both clinical and research settings. The classification will provide a more refined lens through which we can interpret the complexities of brain functionality and structure and understand what makes a brain mildly traumatically injured or not.

4. Classification Methods

Building upon the foundations laid in the previous chapter, where we meticulously analyzed data preprocessing and scrutinized brain networks, we now venture into the critical phase of applying this knowledge to develop robust classification methods. The objective at this juncture is clear: to craft a sophisticated framework capable of distinguishing between healthy controls and individuals suffering from mild traumatic brain injuries (mTBI), utilizing the rich data encapsulated in graphs.

In this chapter, we will explore a selection of classification methodologies, each harboring the potential to accurately segregate individuals based on the intricate patterns and characteristics unearthed in their brain networks. Our goal is to forge a classification model that not only withstands scientific scrutiny but also serves as a beacon for future research in this domain.

As we delve deeper, we aim to seamlessly integrate the insights garnered from our previous analyses, fostering a classification system that epitomizes the synergy of interdisciplinary research. Let us now embark on this pivotal journey, where theory meets application, steering us closer to unraveling the complex narratives woven within healthy and mTBI affected brain networks.

4.1 Support Vector Machines (SVM)

Support Vector Machines (SVMs) are a set of powerful supervised learning methods used for classification, regression, and outliers detection. They are particularly effective in high-dimensional spaces, which makes them a suitable tool for brain network analysis, where the complexity and dimensionality of the data are often high. (Kepl et al., 2022)

Mathematical Foundation. The core principle of SVM is to map the data into a higher-dimensional space and find the optimal hyperplane that distinctly categorizes different classes in this space. The mathematical formulation of SVM can be described as follows:

Given a training set of instance-label pairs (x_i, y_i), where $x_i \in R^n$ and $y_i \in \{-1, 1\}$, the SVM seeks to find the optimal separating hyperplane by solving the following optimization problem:

$$minimize \quad \frac{1}{2}\|w\|^2 + C\sum_{i=1}^{n} \xi_i$$

$$subject\ to \quad y_i(w \cdot x_i + b) \geq 1 - \xi_i, \xi_i \geq 0, i = 1, ..., n$$

Here, w is the normal vector to the hyperplane, b is the bias term, C is a regularization parameter, and ξ_i are slack variables that allow for misclassification of data points but penalize them in the objective function. The decision function that classifies new instances is given by:

$$f(x) = sign(w \cdot x + b)$$

Kernel methods can be employed to handle non-linearly separable data, where the dot product in the feature space is replaced by a kernel function.

Application in Brain Network Analysis. In the realm of brain network analysis, SVMs can be instrumental in classifying different states or conditions, such as distinguishing between healthy controls and mTBI patients. The features used for classification are derived from graph theoretical metrics computed from the adjacency matrices representing the brain networks.

The SVM will be trained on features such as nodal strength, global efficiency, characteristic path length, modularity, rich club coefficient, assortativity, and betweenness centrality, which were discussed in the previous chapter. These features encapsulate vital information about the structural and functional aspects of brain networks, offering a rich dataset for SVM analysis.

SVMs stand out for their ability to handle high-dimensional data effectively and their robustness against overfitting, especially when the number of training samples is limited.

4.2 K Nearest Neighbors (k-NN)

The K-Nearest Neighbors (k-NN) algorithm is a type of instance-based learning, where the algorithm doesn't explicitly learn a model. Instead, it opts to memorize the training instances which are subsequently used as "knowledge" for the prediction phase. This method is particularly useful in cases where the data patterns are hard to describe with a mathematical model.

Mathematical Foundation. The k-NN algorithm operates on a very simple principle. Given a new, unknown observation, it searches the training set for the k-training examples that are closest to the observation and returns the most common output value among them. The distance between observations can be measured using various metrics such as Euclidean, Manhattan, or Minkowski distance. Mathematically, the Euclidean distance, which is used in this research, between two points *x* and *y* in a *n*-dimensional space is calculated as:

$$d(x, y) = \sqrt{\sum_{i=1}^{n} (x_i - y_i)^2}$$

Application in Brain Network Analysis. In the context of brain network analysis, k-NN can be employed to classify different groups, such as distinguishing between healthy controls and mTBI patients, based on the features extracted from brain networks. These features, including nodal strength, global efficiency, and modularity, among others, encapsulate vital information about the structural and functional aspects of brain networks. The k-NN algorithm can be particularly adept at identifying subtle patterns in this high-dimensional feature space, which might be overlooked by other algorithms.

While SVMs are known for their efficacy in high-dimensional spaces and their ability to find complex decision boundaries, k-NN offers simplicity and the ability to adapt quickly to changes. However, it might suffer from the curse of dimensionality, and the choice of an appropriate value for k and the right distance metric is crucial for its performance. Moreover, unlike SVMs, k-NN is more

computationally intensive during the testing phase, as it requires the computation of distances between the test instance and all training instances.

4.3 Convolutional Neural Network (CNN)

In the evolving landscape of brain network analysis, the application of advanced machine learning techniques, particularly Convolutional Neural Networks (CNNs), has emerged as a promising approach. CNNs, a category of deep learning algorithms, have demonstrated remarkable efficacy in image and video recognition, among other tasks. When applied to brain network analysis, CNNs can classify adjacency matrices derived from MEG data as images, thereby potentially automating the diagnosis and study of mTBI.
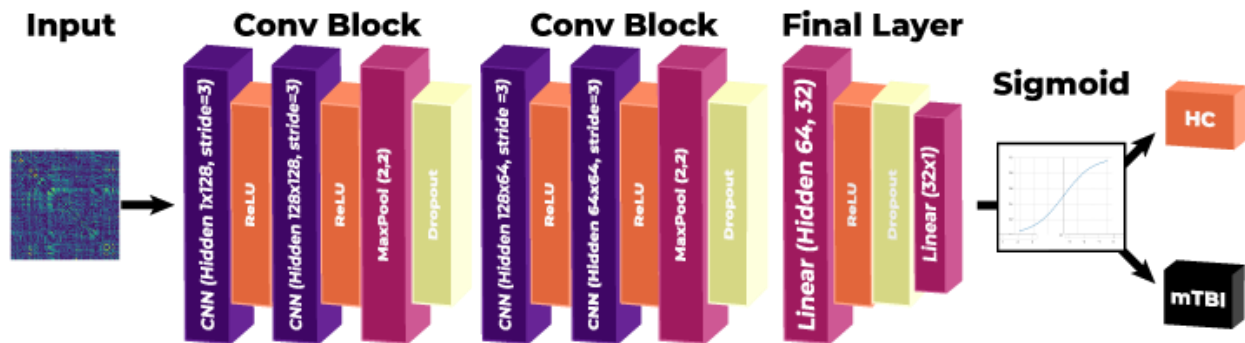
Figure 4.1 The architecture of the CNN used.

Structure and Functioning of CNNs. CNNs are structured to learn spatial hierarchies automatically and adaptively from data, making them highly suitable for image classification tasks. A standard CNN architecture consists of three primary layers: the *convolutional* layer, the *pooling* layer, and the *fully connected* layer.

- The **convolutional layer** applies various filters to the input data, creating feature maps that highlight different aspects of the data.

- The **pooling layer** reduces the dimensionality of each feature map while retaining the most essential information.

- The **fully connected layer** utilizes this information to classify the input data into various categories.

In the context of brain network analysis, the adjacency matrices, which encapsulate the statistical dependencies between different brain regions, can be treated as images, on which our CNN can be trained. These matrices serve as the input data for the CNN, providing a rich source of data for the CNN to analyze and learn from. The architecture of the CNN's model we used in our research consists of two convolutional blocks followed by a final classifier, as shown in **Figure 4.1**. The chosen architecture is a suggestion made in the publication of Klepl et al. (2022), since it was the most efficient one in their study, and it was a result of hyperparameter tuning.

Each block houses a pair of convolutional layers with a stride of 3, succeeded by layers for maximum pooling and dropout. The final classifier is formulated with a duo of linear layers, separated by a dropout layer. The initial block is equipped with 128 convolutional filters, escalating to 64 in the subsequent block. Concurrently, the linear layers maintain a hidden size of 32. A dropout rate of 0.1 was selected for neuron elimination during the process.

The ReLU function was the preferred choice for activation, owing to its computational agility and efficacy in steering the training of deep networks, thereby alleviating potential issues of vanishing gradients commonly associated with sigmoid or tanh functions in extensive networks. Contrarily, the terminal layer adopted the sigmoid function as the activation medium, a strategy renowned for its success in binary classification endeavors, hence its prevalent utilization in such contexts.

Besides the activation function and the number of convolutional filters in each layer, there are other hyperparameters, too, that are used as configurations of the network, aiming to structure and tune its performance. They play a critical role in the behavior of the CNN and can significantly impact the effectiveness and efficiency of the learning process. The hyperparameters chosen for use were:

- **Learning Rate**: The learning rate is a hyperparameter that controls how much the model's weights should be updated during training. A higher learning rate might lead to rapid learning but can overshoot the optimal solutions, while a too-low learning rate can cause the learning process to be slow and potentially get stuck in local minima. Finding an appropriate learning rate is essential for efficient and effective model training.

- **Batch Size**: Batch size refers to the number of training samples used in one iteration of the model training, that is, the number of samples after which the model's weights are updated. A smaller batch size can lead to a more stable convergence by providing more frequent weight updates, but it can also result in a noisy gradient. Conversely, a larger batch size offers a more accurate estimate of the gradient but requires more memory and can result in slower convergence.

- **Weight Decay**: Weight decay, often associated with regularization, is a technique to prevent overfitting by penalizing large weights. It works by adding a term to the loss function that involves the L2 norm of the weights, effectively shrinking them during training. This can lead to a simpler and more generalizable model that performs better on new, unseen data.

- **Gamma Rate**: Gamma rate is typically associated with learning rate schedulers, particularly in methods such as exponential decay, where the learning rate is multiplied by a factor (gamma) at regular intervals. The gamma rate determines how quickly the learning rate decreases over time. Adjusting the gamma rate helps in controlling the learning process, allowing for a fast initial learning phase and then a gradual slowing down to fine-tune the model parameters.

Selecting the appropriate hyperparameters is often a crucial step in designing a CNN model that can learn generalized patterns effectively.

The classification process entailed dividing the data into three distinct subsets: 60% for training, 20% for validation, and the remaining 20% for testing. The training and validation sets were utilized during the model's training phase, with the testing set reserved for the final evaluation phase. During training, the model received the training dataset and adjusted its parameters, such as the weights in the convolutional layers, based on the comparison between its predictions and the actual targets. Subsequently, the model was evaluated using the validation dataset, which had not been previously seen by the model. The accuracy achieved on the validation dataset provided a measure of confidence in the model's ability to generalize well. Upon the completion of the training phase, the model was subjected to the test dataset to assess its performance on entirely new data.

Additionally, to enhance the training process, the technique of early stopping was implemented. Specifically, training would cease if the validation loss did not improve for 15 consecutive epochs, thereby mitigating the risk of overfitting. The upper limit for the number of epochs was set at 300, ensuring the model had ample opportunity to learn from the data without the detriment of excessive training.

4.3.1 Hyperparameters Tuning

The selection of the remaining hyperparameters was facilitated automatically through the **Hyperopt Python library** (Bergstra et al., 2013). Hyperopt is a meta-modeling approach to support automated hyperparameter optimization, thus providing practical tools that are too random such as Random Search, or too exhaustive, such as Grid Search, with a reproducible and unbiased optimization process. It uses a Bayesian approach to find the best values for the hyperparameters.

To use it, 4 key things for our model need to be specified:

- The **Objective function**, which is the value needed to be minimized during the computation. In this thesis, this is the *minus average validation accuracy score*, that results from a k-fold cross validation.

- The **Search scope**, which is the range of values a given hyperparameter can take.

- The **Tuning algorithm**. Hyperopt supports two main algorithms, *Random Search* and *Tree of Parzen Estimators* (Bayesian) (Bergstra et al., 2011). In the thesis, the latter is used, as it is known to produce the best results.

- The **Evaluations**, which refers to the number of different hyperparameters instances to train the model over. It is suggested to be 10-30 times the number of hyperparameters defined in the search space, to optimize for performance and computation time.

The **Tree of Parzen Estimators (TPE)** algorithm as already mentioned, is a method for hyperparameter optimization that belongs to the family of Bayesian optimization algorithms. TPE models the probability distribution of hyperparameters given the likelihood of those hyperparameters to yield good performance measures. It constructs a probabilistic model that places higher probability on hyperparameters that improve the model's performance and lower probability on those that perform poorly. The algorithm iteratively selects new hyperparameter sets to evaluate by choosing values that maximize the expected improvement over the current best result.

The application of CNNs in this context is expected to unveil intricate patterns and connections that might be less apparent or overlooked in traditional analysis methods. Moreover, the CNN approach aligns with the broader trend of leveraging machine learning algorithms to enhance the accuracy and efficiency of medical diagnoses and research.

4.4 Graph Convolutional Network (GCN)

In the rapidly advancing field of brain network analysis, the integration of Graph Neural Networks (GNNs) and Graph Convolutional Networks (GCNs), a sophisticated machine learning technique, stands as a beacon of innovation. GNNs, a subset of deep learning algorithms, have showcased significant prowess in tasks such as social network representation and molecular structure analysis. In the realm of neuroscience, these networks offer a promising avenue for the analysis of brain networks, particularly in distinguishing between different states of brain health.

Mathematical Background. The GCN, a variant of GNN, operates based on a message-passing framework, which fundamentally assumes that neighboring nodes in a graph should have similar features. Mathematically, the operation of a GCN layer can be represented as:

$$H^{(l+1)} = \sigma\left(D^{-\frac{1}{2}}AD^{-\frac{1}{2}}H^{(l)}W^{(l)}\right)$$

where:

- $H^{(l)}$ is the matrix of node features at layer l,

- A is the adjacency matrix representing the graph structure,

- D is the diagonal degree matrix,

- $W^{(l)}$ is the weight matrix at layer l,

- σ is a non-linear activation function.
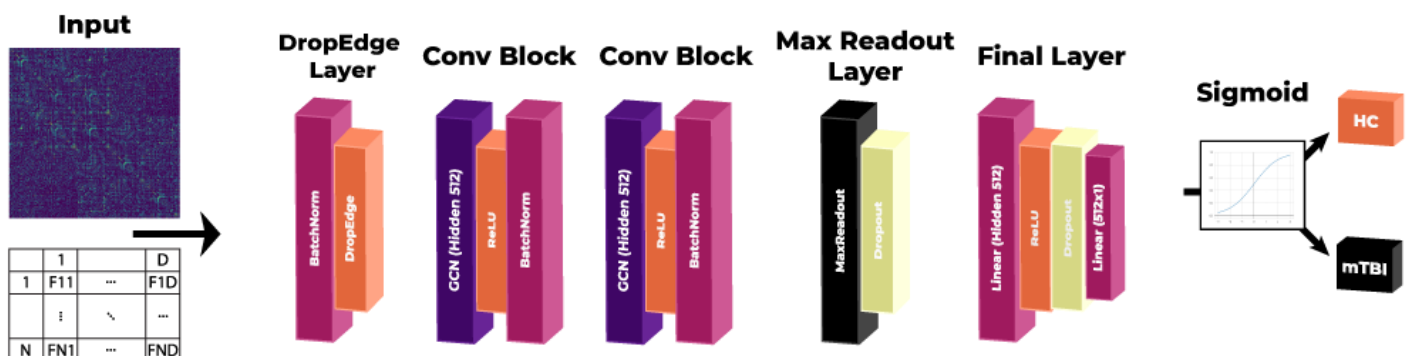
Figure 4.2 *The architecture of the GCN used.*

Structure and Functioning of GCN. GNNs are designed to automatically and adaptively learn the topological patterns present in graph data, making them an ideal choice for the classification of brain networks represented as graphs. In our study, we are going to build a GCN, a specialized type of neural network designed to work directly with graphs. The network takes two inputs: a *weighted adjacency matrix* representing the connections between nodes, and a *node feature matrix* representing the characteristics of each node. Bellow, the architecture of this GCN is described:

1. **Input Preparation**: Initially, the node feature matrix undergoes a normalization process to make the data more manageable for the network.

2. **Drop-Edge Layer**: Before entering the main layers of the network, the adjacency matrix goes through a "Drop-Edge" layer, where some connections (edges) between nodes are randomly removed. This step helps in making the model more robust by preventing overfitting.

3. **Hidden Layers**: The core of the network consists of two hidden layers, where the actual computation happens. These layers can capture the complex patterns in the data. After each of these layers, a normalization process is applied again to stabilize the activations.

4. **Max Readout Layer**: After the hidden layers, a "Max Readout" layer is applied, which essentially picks the most significant information from the nodes, helping in reducing the dimensionality of the data.

5. **Fully Connected Layers**: Following the max readout, the data is passed through a series of linear layers where further computation happens. These layers are interspersed with dropout layers (to prevent overfitting) and activation functions to introduce non-linearity into the model.

6. **Output Layer**: Finally, the data reaches the output layer where it is passed through a sigmoid function. This function squishes the output values between 0 and 1, providing us with the probabilities which are used for classification.

The structure of the GCN is shown in **Figure 4.2**. The chosen architecture is a suggestion made in the publication of Klepl et al. (2022), since it was the most efficient one in their study, and it was a result of hyperparameter tuning. The hidden layers incorporated in the architecture of the GCN model consist of 512 convolutional filters. The same number of filters is applied to the linear layers. The Drop-Edge layer, implemented prior to the hidden layers, randomly discards graph edges with a 20% probability, whereas the dropout mechanism within the Fully Connected layer is set to a high rate of 0.9. Alongside these hyperparameters, the GCN configuration also includes the following parameters:

- **Learning Rate**

- **Weight Decay**

- **Gamma Rate**

Notably, the Batch Size for the GCN is fixed at 1, due to the limitation that the GCN cannot process multiple graphs simultaneously. An alternative approach, involving the construction of a shared adjacency matrix with variable node features, would be impractical and computationally inefficient for our dataset. Once again, the HyperOpt tool helped refining the hyperparameter values.

The application of GNN/GCN in the analysis of brain networks represents a significant advancement in neuroscience research. By leveraging the rich information encapsulated in brain graphs, these networks can potentially uncover intricate patterns and associations that are indicative of specific brain states or conditions. In the context of MTBI, this approach holds promise in identifying subtle alterations in brain network dynamics, which traditional methods might overlook. Moreover, the utilization of graph metrics as features provides a multi-faceted view of brain networks, potentially leading to more accurate and robust classifications.

5. Results and Discussion

In this final chapter of this thesis, we delve into a comprehensive analysis and discussion of the results obtained from our research. The primary focus of this discussion revolves around the classification methods utilized, namely Support Vector Machines (SVM), k-Nearest Neighbors (kNN), Convolutional Neural Networks (CNN), and Graph Convolutional Networks (GCN). These methods were employed to assess the performance of our brain network classification model, which incorporated various network topologies and training strategies.

Notably, SVM, kNN, and CNN exhibited remarkably consistent results, hovering around 86% accuracy when trained on both the aggregated single layer and the multilayer topology. However, intriguingly, the utilization of the full multilayer topology led to more variable outcomes, ranging from 50% to 70%. The most notable achievement in the research came from the implementation of GCNs, where classification results reaching an impressive 97% were witnessed. This remarkable performance underscores the potential of GCN in brain network analysis and classification tasks.

In the pages that follow, we will discuss the intricacies of our training methodologies, parameter selections, and result extraction techniques. Our aim is to offer a comprehensive understanding of the factors influencing classification outcomes and provide insights that may inform future research endeavors in the field of brain network analysis.

Results

As already mentioned, the results of the classification methods' application obtained were at most cases good, even achieving near-perfect classification (GCN – 97%). In this section, the procedure followed to receive these results will be described.

Support Vector Machine

The Support Vector Machine (SVM) Classifier in our study underwent training using three distinct sets of features. Initially, it was trained on a comprehensive set of graph features, as detailed in **Chapter 3.5.2**, encompassing *mean nodal strength, characteristic path length, global efficiency, betweenness centrality, modularity, mean participation coefficient, and assortativity*. Subsequently, a separate classifier was trained solely on the node strengths of each node's signal, representing nodes with the strongest connections and their associated connections. Lastly, another classifier was trained using the betweenness centralities of each node, indicating the importance of a node in terms of its connections within the network.

The training process was carried out using a cross-validation technique, a statistical method employed to evaluate a predictive model's performance and generalizability. To ensure robustness, this process was repeated multiple times, following a 5-fold cross-validation strategy. This rigorous approach prevented overfitting and provided a reliable assessment of the model's accuracy and ability to perform effectively on unseen data.

In our study, this cross-validation procedure was executed 300 times for each combination of estimator, topology, and features. The ensuing results of this extensive procedure are presented below:

Table 5.1 | *Accuracies achieved by the SVM models*

Aggregated Topology	*All Features*	*Nodal Strength*	*Centralities*
IPLV	0.6916 ± 0.1096	**0.8488 ± 0.0765**	0.8043 ± 0.0937
MI	0.5948 ± 0.1126	**0.8887 ± 0.0823**	0.7468 ± 0.1075
AEC	0.5500 ± 0.0852	**0.8694 ± 0.0796**	0.7778 ± 0.1030

Multiplex Topology	All Features	Nodal Strength	Centralities
IPLV	0.7384 ± 0.1057	**0.8450 ± 0.0914**	0.5429 ± 0.1040
MI	0.6108 ± 0.1161	**0.8724 ± 0.0809**	0.5960 ± 0.1076
AEC	0.4716 ± 0.0429	**0.8081 ± 0.0901**	0.6197 ± 0.1069

Full Multilayer Topology	All Features	Nodal Strength	Centralities
IPLV	**0.5723 ± 0.1237**	0.5309 ± 0.1109	0.5409 ± 0.0920
MI	0.4956 ± 0.0956	**0.5749 ± 0.1074**	0.5136 ± 0.0334
AEC	0.4738 ± 0.0509	0.5027 ± 0.1164	**0.5033 ± 0.0128**

It is easy to observe that in most cases the classification achieved a high accuracy (>80%) when the SVM was trained on the **Nodal Strength** of the nodes, with the highest being extracted from the **Mutual Information (MI)** adjacency matrix when the **single aggregated layer topology** was enforced.

Also worth mentioning is the fact that when the Full Multilayer Topology was applied, the classification wasn't accurate achieving at most a 57,49%. This result might be expected, as the features derived from the Full Multilayer FC matrix may not be as discriminative for the classification task at hand.

Considering the topologies, the **Multiplex Topology** tends to yield higher accuracy for all estimators when using *all features* and *node strengths*, which might indicate that this approach to modeling the network preserves important discriminative information that is beneficial for the SVM model's performance.

A permutation t-test was additionally performed on the matrix corresponding to the feature set/topology/estimator combination with the highest accuracies, for each estimator, to assess the significance of individual features. The permutation test on the case of the MI in the single aggregated layer topology showed this result:

Table 5.2 | *Features with high importance according to permutation t-test*

Nodal Feature	p-value	t-statistic
Fusiform_R	2.44E-06	-4.740505526
Paracentral_Lobule_L	1.72E-10	-6.45174395
Precentral_R	7.59E-16	-8.195646604
Precuneus_L	1.80E-23	-10.24047867
Postcentral_R	5.75E-38	-13.43857541
Temporal_Pole_Mid_R	5.02E-49	-15.55614955
Heschl_R	0	-96.26986642
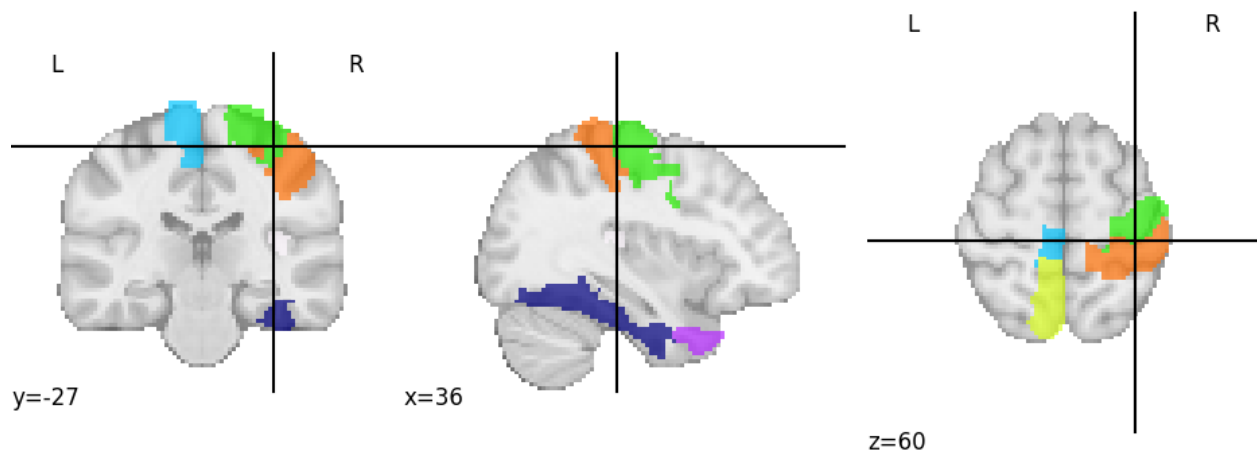
Figure 5.1 *The Regions of Interest having the greatest statistical importance.*

Out of the 90 features, only 7 successfully passed the importance test, with the **Right Heschl node strength** being the most significant. In contrast, for other estimators and topologies, nearly all features exhibited importance. A noteworthy finding was that the majority of the most crucial features across all cases were associated with the **theta frequency band**.

k-Nearest Neighbors

The approach employed for the k-Nearest Neighbors classification method closely resembled that of the SVM models. However, a distinct step was introduced into the process. Prior to the 300 iterations of 5-fold cross-validation, an exhaustive algorithm was applied to determine the optimal value of k. This search encompassed values from 1 to 31, utilizing the mean accuracy from a 5-fold cross-validation as the basis for selection. The results shown below also include the best k value chosen.

Table 5.3 | *Accuracies achieved by the kNN models*

Aggregated Topology	All Features	k	Nodal Strength	k	Centralities	k
IPLV	0.7882 ± 0.0928	10	**0.8579 ± 0.0867**	**5**	0.8264 ± 0.0886	25
MI	0.6187 ± 0.1015	4	**0.8718 ± 0.0869**	**5**	0.8523 ± 0.0809	3
AEC	0.6054 ± 0.1092	18	**0.8872 ± 0.0759**	**2**	0.8104 ± 0.0922	10

Multiplex Topology	All Features	k	Nodal Strength	k	Centralities	k
IPLV	0.7814 ± 0.0941	15	**0.8329 ± 0.0932**	**5**	0.5649 ± 0.1088	4
MI	0.6686 ± 0.1126	13	**0.8780 ± 0.0758**	**1**	0.5836 ± 0.0910	7
AEC	0.4893 ± 0.1137	5	**0.7725 ± 0.1065**	**8**	0.5868 ± 0.1040	29

Full Multilayer Topology	All Features	k	Nodal Strength	k	Centralities	k
IPLV	**0.6182 ± 0.1095**	**3**	0.5769 ± 0.1171	5	0.6039 ± 0.0941	30
MI	0.5198 ± 0.0963	24	**0.6193 ± 0.1183**	**6**	0.5628 ± 0.1068	3
AEC	**0.5979 ± 0.1084**	**10**	0.5320 ± 0.0543	26	0.5359 ± 0.0810	1

The outcomes are comparable to those obtained with SVM models, with a marginal improvement. The peak accuracy is realized using the AEC estimator within the simple aggregated layer topology, specifically when utilizing the Nodal Stengths feature set. Similarly, the Full Multilayer topology also yields the least accurate results in this analysis. Overall, IPLV appears to consistently provide higher accuracy across all topologies and feature sets, indicating that features derived from IPLV are more discriminative for k-NN classification in this context.

Furthermore, the optimal k values vary significantly across the estimators and features, reflecting the importance of neighborhood size in the classification process. These values though do not surpass the value of 10 regarding the optimal values of each topology, indicating that in the best scenarios, the classification is more sensitive to the immediate neighbors.

A permutation t-test was conducted once more to identify the most significant features. The p-values obtained indicated that all features are important for the classification task. Notably, when employing the MI and AEC estimators within the straightforward aggregated layer topology, the Right Heschl Nodal Stength emerged as the most significant feature, suggesting that this brain region may play a key role in distinguishing between mTBI patients and healthy individuals.

Convolutional Neural Networks

For the Neural Networks, the training process did not involve feature extraction. The CNN used as input the Functional Connectivity matrix of each sample. After the data normalization for standardization and generalization, the hyperparameters tuning took place. The range of values each hyperparameter was set to be searched were:

- **Learning Rate**: a value in the uniformly distributed range between e^{-10} and e^{-4}.

- **Batch Size**: a discrete value in the uniformly distributed range between 3 and 6. Since the total samples were 60, and thus, in the 5-fold cross-validation the size of the test input was 6, this value should not surpass the test input size.

- **Weight Decay**: a value in the uniformly distributed range between e^{-10} and e^{-4}.

- **Gamma rate**: a value uniformly distributed range between 0.8 and 1.

The hyperparameter tuning, although time-consuming, provided us the optimal values, in a run of 40 evaluations. Bellow you can see the results:

Table 5.4 | *The optimal hyperparameter values for topologies-FC estimators by Hyperopt (CNN)*

Topology	FC Estimator	Learning Rate	Batch Size	Weight Decay	Gamma Rate
Single Aggregated Layer	**IPLV**	0.000236064	3	0.000809655	0.941871
Single Aggregated Layer	**MI**	0.00117068	4	0.0000535	0.966507
Single Aggregated Layer	**AEC**	0.00116644	6	0.000931653	0.825818
Multiplex	**IPLV**	0.00018148	4	0.0000475	0.953018
Multiplex	**MI**	0.0000466	4	0.000403813	0.892538
Multiplex	**AEC**	0.0000472	3	0.000294425	0.924925
Full Multilayer	**IPLV**	0.00005	3	0.000435197	0.801115
Full Multilayer	**MI**	0.000302184	6	0.0000478	0.944316
Full Multilayer	**AEC**	0.0000475	3	0.0063897	0.921444

From the table, we can conclude the following:

- The **learning rates** are quite low across all topologies and functional connectivity (FC) estimators, which suggests that a gentle approach to updating the weights is optimal for this classification task. It also implies that the data or the classification problem may be sensitive to adjustments in the model's weights, requiring careful tuning.

- The **weight decay** values are also quite low, which suggests that only slight regularization is necessary. This might indicate that the model is less prone to overfitting or that the data has sufficient complexity that it does not require aggressive regularization. However, as shown later, there were times that the validation loss differed from the training loss by a significant amount, indicating that in these certain cases overfitting might have been noticed.

- The **gamma rates** values suggest a moderate decay rate for the learning rate during training, ensuring that the learning rate is reduced over time but not too abruptly.

The careful tuning of these values shows the complexity of the machine learning models and their dependency on correctly selected hyperparameters. It is also apparent that the utilization of optimization libraries like HyperOpt enhances the models' performance through picking the appropriate hyperparameters.

After finding the optimal hyperparameter values, a 5-fold cross validation was run 5 times, to verify the results and to keep track of other information regarding the CNN training. Below these results are displayed.

Table 5.5 | *Accuracies achieved by the CNN models.*

	Single Aggregated Layer	*Multiplex*	*Full Multilayer*
IPLV	0.8933 ± 0.0828	0.8633 ± 0.0802	**0.7067 ± 0.1026**
MI	**0.9133 ± 0.0582**	**0.8767 ± 0.0809**	0.5300 ± 0.1175
AEC	0.8733 ± 0.0739	0.8567 ± 0.0791	0.6800 ± 0.1151

The highest accuracy was attained using the Mutual Information (MI) estimator within the Single Aggregated Layer topology, whereas the lowest accuracy was observed with the same FC estimator applied to the Full Multilayer topology. The Multiplex topology demonstrated accuracy approximately on par with the Single Aggregated Layer topology, indicating that it could play a significant role in the classification of healthy controls and mTBI patients.

Some interesting conclusions can also be derived from the Loss vs Epoch and the Accuracy vs Epoch figures (**Figure 5.2**). IPLV generally shows a closer alignment between training and validation losses, suggesting it might be a more robust estimator for this classification task. The Full Multilayer topology tends to show higher losses and potential overfitting issues across all FC estimators, which is consistent with the lower classification accuracies observed in the earlier table.
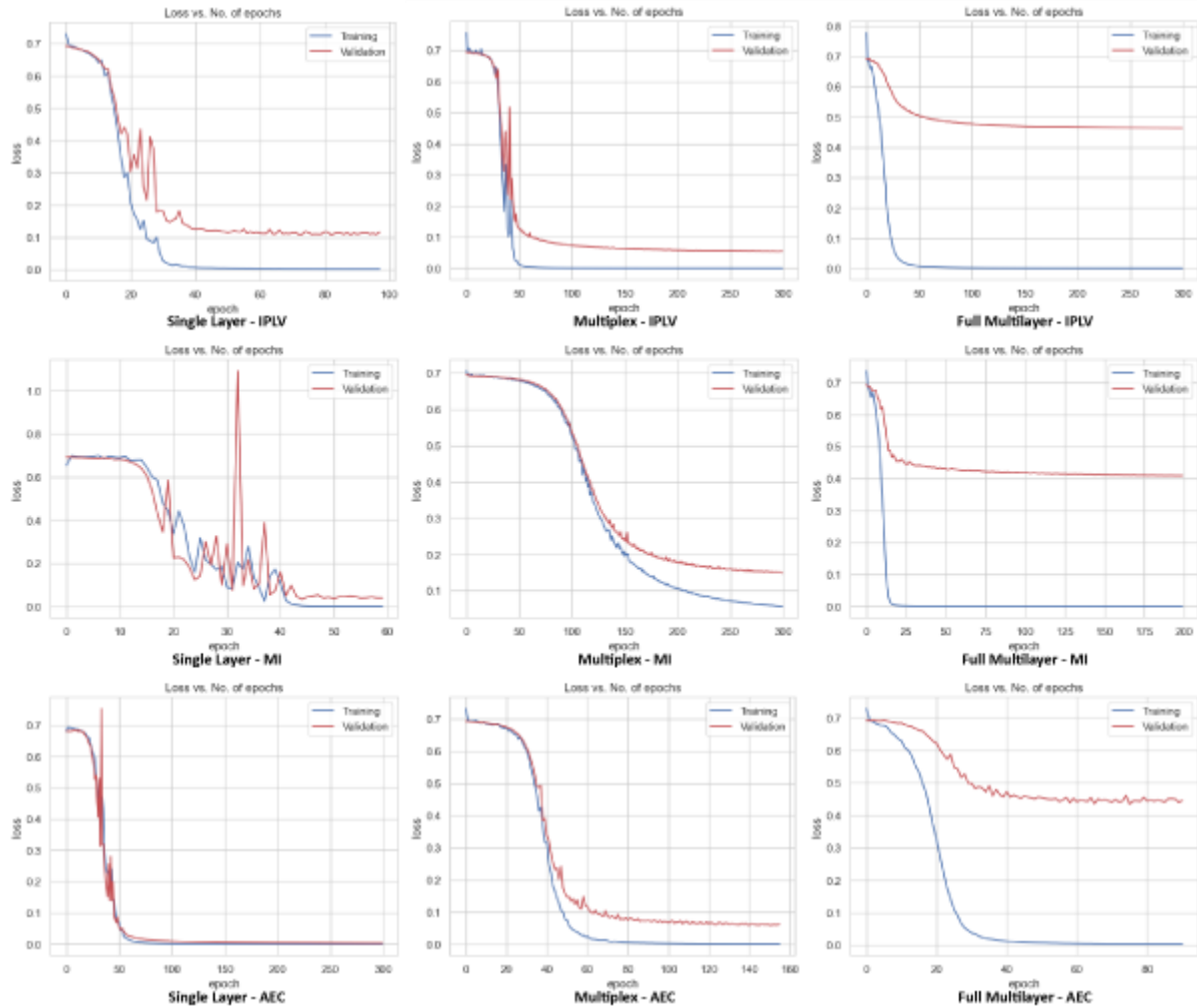
Figure 5.2 *CNN Training and Validation loss over the number of epochs trained on different FC estimators and topologies.*

Some comments we could conclude to from these figures are:

- At most cases, the training and validation loss both decrease smoothly and remain close together throughout the training, indicating that the model is generalizing well in these cases.

- The figures derived from the Full Multilayer topology show a significant gap between the training and validation loss, indicating a potential overfitting issue a model that does not generalize as well as in other topologies. The validation loss is also considerably higher compared to other topologies. These observations align with the lower classification accuracies seen for the Full Multilayer topology.

- In many cases, early stopping seems to have taken effect, as the number of epochs is less than the maximum 300, suggesting the model converged quickly.

- When using MI in the Single Aggregated Layer topology, the training loss shows more fluctuation, but overall, it decreases well. The validation loss shows some instability, which might suggest a model that is less stable or has a harder time generalizing compared to the IPLV estimator.

In general, comparing these results to the previously discussed SVM and k-NN models, it is evident that the CNN models achieve varying levels of accuracy depending on the FC estimator and topology used. The Single Aggregated Layer topology generally provides the highest accuracies across all estimators when implemented in CNN models, similar to what was observed with the SVM and k-NN methods. This consistency across different classification approaches emphasizes the potential suitability of the Single Aggregated Layer topology for HC/mTBI classification tasks.

Graph Convolutional Network

The training procedure for the GCN is analogous to that of the CNN model. In initial phase of the process, feature extraction is applied to the original MEG signals, with the specific features outlined in **Section 3.5.3**. For the investigation of the single layer topology, we utilized the unfiltered signals, which yielded an array comprising 9 features for each of the 90 nodes. In contrast, for all other scenarios, the filtered signals were employed, generating an array consisting of 9 features across 450 nodes, equating to 90 nodes for each of the five frequency bands.

Subsequently, the HyperOpt tool helped refining the hyperparameter values through a series of evaluations equal to 30. The hyperparameter values computed are presented below:

Table 5.6 | *The optimal hyperparameter values for topologies-FC estimators by Hyperopt (GCN)*

Topology	FC Estimator	Learning Rate	Weight Decay	Gamma Rate
Single Aggregated Layer	**IPLV**	0.000146059	0.00448692	0.879547
Single Aggregated Layer	**MI**	0.000369024	0.000310777	0.864897
Single Aggregated Layer	**AEC**	0.00110464	0.000618038	0.902186
Multiplex	**IPLV**	0.0000476	0.000137086	0.807579
Multiplex	**MI**	0.000666004	0.000307109	0.829866
Multiplex	**AEC**	0.00112024	0.000788121	0.832246
Full Multilayer	**IPLV**	0.000816	0.00711633	0.804472
Full Multilayer	**MI**	0.000140931	0.0018564	0.809759
Full Multilayer	**AEC**	0.00437827	0.00047582	0.826545

The Learning Rates and the values of the Weight Decay are different across all topologies and estimators. These variations suggest that each combination of topology and estimator may require a specific learning rate and decay of weights for optimal training of the GCN. The highest value of both hyperparameters was observed for the AEC estimator in the Full Multilayer topology, potentially indicating a greater need for regularization in this configuration, fact supported by the accuracy results bellow. The Gamma Rates are similar across the configurations (in the range of 0.8 to 0.9), so a moderate reduction in the learning rate was required over time. Once again, the careful consideration and tuning is required to develop effective models, maximizing the GCN's performance for the classification task.

Once optimized, the GCN model undergoes training 20 times, employing a 5-fold cross-validation method to ensure robustness and reliability in its predictive performance.

***Table 5.7** | Accuracies achieved by the GCN models.*

	Single Aggregated Layer	Multiplex	Full Multilayer
IPLV	**0.9692 ± 0.0397**	**0.7533 ± 0.1080**	**0.7667 ± 0.0994**
MI	**0.9683 ± 0.0401**	0.6633 ± 0.1253	0.5633 ± 0.1356
AEC	**0.9692 ± 0.0393**	0.5067 ± 0.0441	0.5067 ± 0.0333

From the results, the following observations can be made:

- The accuracies for IPLV, MI and AEC are almost identical for the Single Aggregated Layer and represent the highest performance across all topologies, suggesting that this topology is highly effective for both estimators when used with GCNs.
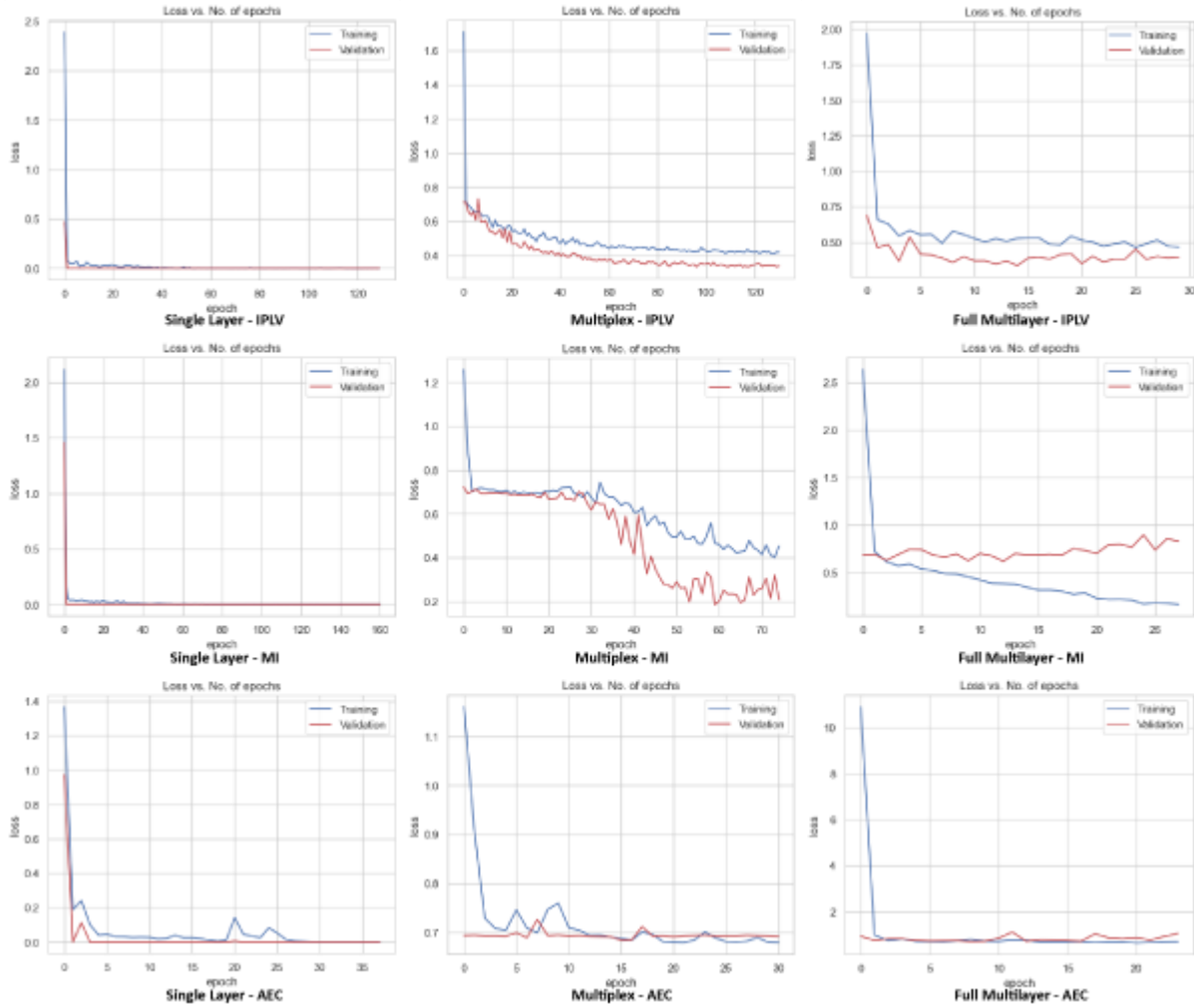

***Figure 5.3** GCN Training and Validation loss over the number of epochs trained on different FC estimators and topologies.*

- A significant drop in accuracy is observed for all estimators for the Multiplex and the Full Multilayer topologies, with IPLV showing the highest accuracy, followed by MI, and AEC performing the least effectively. This suggests that both topologies may present more challenges for the GCN models to capture the discriminative features necessary for classification. The Full Multilayer topology seems to be the least suitable when used with GCNs, as indicated by the consistent accuracies for AEC and the drop for MI.

Variations in the performance of models trained on the Single Layer versus Multilayer topologies can be primarily attributed to the methods employed for feature extraction. The findings suggest that features derived from the original signals significantly aid the model in differentiating between Healthy Controls and mTBI patients, achieving near-perfect classification rates. However, the same level of distinction is not observed with features from the filtered signals. Consequently, it may be necessary to either identify new features more suited to the Multilayer topologies or enhance the GCN architecture by incorporating a larger number of Graph Convolutional filters. This is because the multilayer Functional Connectivity (FC) Brain Networks contain an abundance of information, which may require a more sophisticated model structure to effectively decode and utilize for classification purposes. Such outcomes can be supported by the high losses that the models provided in the multilayer topologies.

Comparing these results to the previous models' accuracies, GCN models appear to outperform them when using Single Aggregated Layer topology. For the rest topologies, while the results using the IPLV estimator seem to be promising, the case for the MI and the AEC seem to be extremely low, and thus inadequate for this classification task. As previously mentioned, it is plausible that with optimized configurations, improved accuracies could be realized. This hypothesis is grounded in the observation that even with a relatively modest setup, one of the three estimators demonstrated satisfactory performance. This suggests that there is potential for further enhancement of the model's accuracy through careful refinement of its configuration.

Figure 5.8 | *Top 10 Performing Models*

Model	Topology	FC Estimator	Accuracy	Specificity	Sensitivity
GCN	Single Aggregated Layer	IPLV	**96.92% ± 3.97**	**0.9674**	**0.9621**
GCN	Single Aggregated Layer	AEC	96.92% ± 3.93	0.9783	0.9717
GCN	Single Aggregated Layer	MI	96.83% ± 4.01	0.9744	0.9874
CNN	Single Aggregated Layer	MI	**91.33% ± 5.82**	**0.8527**	**0.9270**
CNN	Single Aggregated Layer	IPLV	89.33% ± 8.28	0.8844	0.9226
SVM (Nodal Stengths)	Single Aggregated Layer	MI	**88.87% ± 8.23**	**0.8892**	**0.8853**
kNN (Nodal Stengths)	Single Aggregated Layer	AEC	**88.72% ± 7.59**	**0.8197**	**0.9509**
kNN (Nodal Stengths)	Multiplex	MI	**87.80% ± 7.58**	**0.8478**	**0.9072**
CNN	Multiplex	MI	**87.67% ± 8.09**	**0.8778**	**0.9850**
CNN	Single Aggregated Layer	AEC	87.33% ± 7.39	**0.8673**	**0.8881**

Overall, most models performed well under the various FC estimators and topologies. As expected in advance, the Neural Networks achieved higher accuracies compared to the traditional Machine Learning techniques. SVM models have historically been robust and effective for binary classification tasks, and in our case, they provided a solid baseline for performance. kNN models, which rely on the similarity between feature sets, also demonstrated utility, especially when the optimal number of neighbors (k) was determined through tuning. CNNs leveraged their ability to automatically learn spatial hierarchies of features, yielding good results particularly with the Single Aggregated Layer topology. GCNs, the most recent addition to our model arsenal, took advantage of the graph structure of the data and showed promise in their ability to incorporate the connectivity information inherent in brain network data. The varying performances observed across different models and topologies highlight the complexity of modeling brain data and suggest that there is no one-size-fits-all approach.

From the figure below, several outcomes are obtained. The models using the Single Layer topology with IPLV and MI estimators (both GCN and CNN) are at the top, indicating that they have the

highest true positive rates for the lowest false positive rates. models using the AEC estimator, regardless of the classification method (CNN, kNN), appear lower on the graph, which shows that they have lower true positive rates for the same false positive rates compared to models using IPLV and MI, suggesting that AEC is less effective in this context. The SVM and kNN models, while still providing reasonable performances, generally appear below the GCN and CNN models, indicating that they may not be as effective in this application.
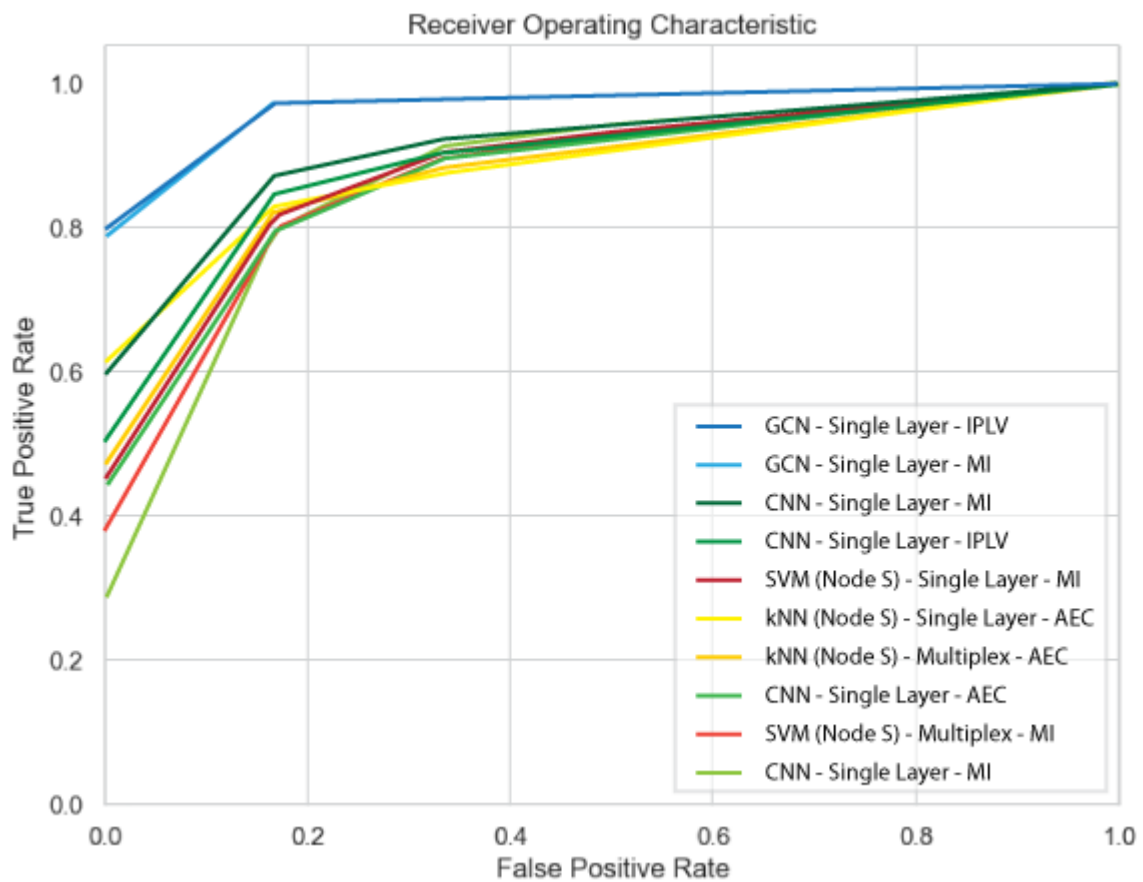
Figure 5.4 *ROC Curves of the top 10 models trained on FC estimators and topologies.*

While each model has shown strengths and limitations, the pursuit of higher accuracy and generalizability remains a central goal. Enhancements to these models, novel approaches to feature selection and extraction, and advanced methods for hyperparameter optimization are some of the techniques that could be enforced to achieve in general higher accuracies. Insights from neuroscience

could guide the development of even more sophisticated models that are not only accurate but also

interpretable within the context of brain function and injury. The integration of these elements will pave

the way for future research to further refine the classification of healthy controls and mTBI patients.

Previous Studies

The landscape of neuroimaging and computational neuroscience is rich with studies aiming to unravel the complexities of the brain, particularly in the context of diagnosing and understanding mTBI. This section delves into a comprehensive comparison between the current study's findings and methodologies and those of previous research in the field.

In the study "*Non-linear Synchronization Methods on Magnetoencephalographic (MEG) Recordings*" by Antonakakis (2015), an examination was conducted into the Cross-Frequency Coupling among specific frequency bands (for example, δ-β, θ-β), employing a methodology akin to the Full Multilayer topology utilized in our thesis. The establishment of Functional Connectivity was achieved through the application of the Phase to Amplitude measure as an estimator between two nodes, either within the same layer or across different layers. Subsequently, models such as k-Nearest Neighbors (kNN), Ensemble (ENS), and Extreme Learning Machine (ELM) were implemented following the application of the tensor subspace analysis (TSA) algorithm. These models yielded the subsequent results.

Figure 5.9 | *Results of 'Non-linear Synchronization Methods on Magnetoencephalographic (MEG) Recordings' research*

Band Coupling	kNN	ENS	ELM
δ, β	91.25 ± 13.24	93.33 ± 11.65	90 ± 8.607
δ, γ1	93.75 ± 6.588	96.67 ± 7.027	76.67 ± 19.56
θ, β	92.5 ± 8.74	90 ±8.607	76.67 ± 21.08
θ, γ1	93.75 ± 10.62	90 ±11.65	83.33 ± 13.61
β, γ2	93.75 ± 10.62	96.67 ±7.027	91.67 ± 8.784
δ, β	91.25 ± 13.24	93.33 ± 11.65	90 ± 8.607
δ, γ1	93.75 ± 6.588	96.67 ± 7.027	76.67 ± 19.56
θ, β	92.5 ± 8.74	90 ±8.607	76.67 ± 21.08
θ, γ1	93.75 ± 10.62	90 ±11.65	83.33 ± 13.61
β, γ2	93.75 ± 10.62	96.67 ±7.027	91.67 ± 8.784

In another study, *Aberrant Whole-Brain Transitions and Dynamics of Spontaneous Network microstates in Mild Traumatic Brain Injury (Antonakakis et al., 2020),* the researchers investigated dynamic functional connectivity (DFC) in mTBI using MEG resting-state recordings to identify abnormal alterations. By reconstructing brain activity across several frequency bands and using phase-locking values for DFC analysis, the research quantified network microstates (NMstates) and assessed group differences using chronnectomics. Classification based on chronnectomics and microstates achieved high accuracy, sensitivity, and specificity as shown bellow.

Figure 5.10 | *Classification Results of 'Aberrant Whole-Brain Transitions and Dynamics of Spontaneous Network microstates in Mild Traumatic Brain Injury' research*

NMstates	Frequency band	Accuracy	Sensitivity	Specificity
NM1	δ	91.27 ± 1.34	100	77.30 ± 3.49
	θ	92.27 ± 1.35	100	80.00 ± 3.49
	α	96.14 ± 0.55	100	90.00 ± 1.42
	β	97.42 ± 0.67	100	93.33 ± 1.74
	γ_{low}	93.85 ± 1.22	100	83.97 ± 3.18
	γ_{high}	96.15 ± 0.65	100	90.00 ± 1.68
NM2	δ	93.56 ± 0.73	100	83.33 ± 1.87
	θ	94.85 ± 0.69	100	86.67 ± 1.83
	α	93.84 ± 0.70	100	83.97 ± 1.88
	β	92.88 ± 0.98	100	81.40 ± 2.53
	γ_{low}	93.85 ± 1.22	100	83.97 ± 3.18
	γ_{high}	95.16 ± 0.54	100	87.40 ± 1.39
Chronnectomics + CI		80.34 ± 1.34	99.65 ± 0.32	49.23 ± 3.56

Another study, *Sensor-level MEG combined with machine learning yields robust classification of mild traumatic brain injury patients (Aaltonen et al, 2023)*, investigated the use of traditional Machine Learning models, specifically Support Vector Machines (SVM), LDA and Logistic Regression (LR) in order to diagnose whether a patient suffers or suffered from MTBI or not. The research achieved median classification accuracies between 80 and 95% without significant differences across methods or datasets, as displayed in the following table.

Figure 5.11 | *Classification Results of 'Sensor-level MEG combined with machine learning yields robust classification of mild traumatic brain injury patients' research.*

Classifier	Experimental Condition	Accuracy (Dataset A-B)
LDA	Eyes Closed	0.95 - 0.85
LDA	Eyes Open	0.34 - 0.29
SVM	Eyes Closed	0.88 - 0.88
SVM	Eyes Open	0.17 - 0.59
LR	Eyes Closed	0.80 - 0.88
LR	Eyes Open	0.12 - 0.45

Finally, the study *Using normative modeling and machine learning for detecting mild traumatic brain injury from magnetoencephalography data* (Itälinna et al., 2023) utilized a machine learning approach with normative modeling on MEG data to detect mTBI. Using a large normative dataset, they modeled individual deviations in MEG signal features, and with support-vector-machine classifiers, they achieved 79% accuracy in distinguishing mTBI patients from controls. The study underscores the potential of this methodology for diagnosing mTBI, highlighting the significance of low-frequency activity in the theta band as an indicator.

Figure 5.12 | *Results of 'Using normative modeling and machine learning for detecting mild traumatic brain injury from magnetoencephalography data' research.*

Normative Data	Accuracy	Sensitivity	Specificity
Full	0.790 ± 0.154	0.912 ± 0.176	0.638 ± 0.277
Age-matched	0.761 ± 0.150	0.907 ± 0.166	0.581 ± 0.277
Random	0.711 ± 0.153	0.914 ± 0.154	0.467 ± 0.318
None	0.786 ± 0.162	0.912 ± 0.154	0.629 ± 0.293

Future Directions

While our study has yielded significant insights into brain network analysis using various classification methods, it also paves the way for promising future research directions. These directions hold the potential to enhance our understanding of brain network dynamics and contribute to the development of more robust diagnostic tools.

One intriguing avenue for future exploration involves extending the multilayer topology across the temporal dimension. Currently, our multilayer analysis focuses on different frequency bands, offering a static snapshot of brain connectivity. To capture the dynamic nature of brain function, researchers may consider implementing a dynamic multilayer approach. This would involve examining how brain networks evolve over time, providing insights into the temporal dynamics of brain function and potential changes associated with brain disorders.

Another interesting direction would be the use of Graph Attention Networks (GATs) instead of the GCN. GATs have gained prominence in recent years for their ability to learn the importance of neighboring nodes in a graph. Integrating GATs into our classification framework could enable more precise feature extraction and classification. By assigning varying attention weights to different brain regions, GATs may reveal subtle but critical patterns in brain connectivity data, potentially leading to improved classification accuracy.

In conclusion, this thesis has laid a strong foundation for future investigations in the field of brain network analysis. These prospective directions, including dynamic multilayer topology, Graph Attention Networks, and the use of other sets of both signal and graph features, hold the promise of advancing our understanding of brain connectivity and enhancing the accuracy of diagnostic tools for neurological conditions. As we embark on these new research journeys, we aim to contribute to the broader scientific community's efforts to unravel the complexities of the human brain.

References

Aaltonen J., Heikkinen V., Kaltiainen H., Salmelin R., Renvall Hanna. (2023). *Sensor-level MEG combined with machine learning yields robust classification of mild traumatic brain injury patients*. Clinical Neurophysiology, Volume 153, Pages 79-87. https://doi.org/10.1016/j.clinph.2023.06.010.

Antonakakis M., Dimitriadis S.I., Zervakis M., Papanicolaou A.C. and Zouridakis G. (2020). *Aberrant Whole-Brain Transitions and Dynamics of Spontaneous Network Microstates in Mild Traumatic Brain Injury*. Front. Comput. Neurosci. 13:90. https://doi.org/10.3389/fncom.2019.00090.

Arnemann K.L., Chen A.J., Novakovic-Agopian T., Gratton C., Nomura E.M., D'Esposito M. (2015). *Functional brain network modularity predicts response to cognitive training after brain injury*. Neurology. 84(15):1568-74. https://doi.org/10.1212/WNL.0000000000001476.

Assistant Secretary, D. O. D. (2007). *Traumatic Brain Injury: Definition and Reporting*. Department of Defense. https://dod.defense.gov/News/Special-Reports/0315_tbi/.

Bahrami M. and Hossein-Zadeh G.-A. (2015), *Assortativity changes in Alzheimer's disease: A resting-state FMRI study,* 2015 23rd Iranian Conference on Electrical Engineering, Tehran, Iran, pp. 141-144, https://doi.org/10.1109/IranianCEE.2015.7146198.

Baniqued P.L., Gallen C.L., Voss M.W., Burzynska A.Z., Wong C.N., Cooke G.E., Duffy K., Fanning J., Ehlers D.K., Salerno E.A., Aguiñaga S., McAuley E., Kramer A.F., D'Esposito M. (2018). *Brain Network Modularity Predicts Exercise-Related Executive Function Gains in Older Adults*. Front Aging Neurosci. 9:426. https://doi.org/10.3389/fnagi.2017.00426.

Banks S.D., Coronado R.A., Clemons L.R., Abraham C.M., Pruthi S., Conrad B.N. & Morgan V.L. (2016). *Altered Structural Brain Networks in TBI Patients with Persistent Post-Concussive Symptoms. Brain Injury*, 30(12), 1461-1471. https://doi.org/10.1080/02699052.2016.1199905.

Battiston F., Nicosia V. and Latora V. (2014) *Structural Measures for Multiplex Networks*. Physical Review E, 89, Article ID: 032804. https://doi.org/10.1103/PhysRevE.89.032804.

Bergstra J., Yamins D., Cox D. D. (2013). *Making a Science of Model Search: Hyperparameter Optimization in Hundreds of Dimensions for Vision Architectures*. TProc. of the 30th International Conference on Machine Learning (ICML 2013), June 2013, pp. I-115 to I-23.

Bergstra, James & Bardenet, R. & Kégl, Balázs & Bengio, Y. (2011). *Algorithms for Hyper-Parameter Optimization*.

Bigler E.D. (2013). *Traumatic brain injury, neuroimaging, and neurodegeneration*. Front Hum Neurosci. https://doi.org/10.3389/fnhum.2013.00395.

Bigler E.D., Orrison W.W., (2004). *Neuroimaging in sports-related brain injury*. In: Lovell, M. R., Echemendia, R.J., Barth, J.T., Collins, M.W. (Eds.), *Traumatic Brain Injury in Sports: An International Perspective*. Lisse, Netherlands, Swets and Zeitlinger, 71–94.

Bigler E.D. & Maxwell W.L. (2012). *Neuropathology of mild traumatic brain injury: relationship to neuroimaging findings*. Brain imaging and behavior, 6, 108-136.

Boccaletti S., Latora V., Moreno Y., Chavez M., Hwang D.-U. (2006). *Complex networks: Structure and dynamics*, Physics Reports, Volume 424, Issues 4–5, Pages 175-308. ISSN 0370-1573. https://doi.org/10.1016/j.physrep.2005.10.009.

Boccaletti S., Latora V., Moreno Y. et al. (2006) *Complex Networks: Structure and Dynamics*. Physics Reports, 424,175. https://doi.org/10.1016/j.physrep.2005.10.009.

Brier M.R., Thomas J.B., Fagan A.M., Hassenstab J., Holtzman D.M., Benzinger T.L. et al. (2013). *Functional connectivity and graph theory in preclinical Alzheimer's disease*. Neurobiol. Aging 35, 757–768. https://doi.org/10.1016/j.neurobiolaging.2013.10.081.

Brookes M.J., Woolrich M., Luckhoo H., Price D., Hale J.R., Stephenson M.C., Barnes S.M., Smith S.M. & Morris P.G. (2011). *Investigating the electrophysiological basis of resting state networks using magnetoencephalography*. Proceedings of the National Academy of Sciences, 108(40), 16783-16788. https://doi.org/10.1073/pnas.1112685108.

Brookes M.J., Tewarie P.K., Hunt B.A.E., Robson S.E., Gascoyne L.E., Liddle E.B., Liddle P.F. and Morris P.G. (2016). *A Multi-Layer Network Approach to MEG Connectivity Analysis*. NeuroImage 132 (May): 425–38. https://doi.org/10.1016/j.neuroimage.2016.02.045.

Buldú J.M. & Porter M.A. (2017). *Frequency-based brain networks: From a multiplex framework to a full multilayer description*. Network Neuroscience, 2(4), 418–441. https://doi.org/10.1162/netn_a_00033.

Bullmore E., Sporns O. (2009). *Complex brain networks: graph theoretical analysis of structural and functional systems*. Nat Rev Neurosci **10**, 186–198. https://doi.org/10.1038/nrn2575.

Carr J., Brown J.M. (2001). *Introduction to Biomedical Equipment Technology.* Prentice-Hall, New Jersey, USA, 4th edition.

Carter A.R., Shulman G.L., Corbetta M. (2012). *Why use a connectivity-based approach to study stroke and recovery of function?* Neuroimage. 62(4):2271-80. https://doi.org/10.1016/j.neuroimage.2012.02.070.

Cassidy J.D., Carroll L.J., Peloso P.M., Borg J., von Holst H., Holm L., Kraus J., Coronado V.G.; WHO Collaborating Centre Task Force on Mild Traumatic Brain Injury. (2004). *Incidence, risk factors and prevention of mild traumatic brain injury: results of the WHO Collaborating Centre Task Force on Mild Traumatic Brain Injury*. https://doi.org/10.1080/16501960410023732.

Combrisson E., Vallat R., O'Reilly C., Jas M., Pascarella A., Saive A., Thiery T., Meunier D., Altukhov D., Lajnef T., Ruby P., Guillot A. and Jerbi K. (2019). *Visbrain: A Multi-Purpose GPU-Accelerated Open-Source Suite for Multimodal Brain Data Visualization*. Front. Neuroinform. 13:14. https://doi.org/10.3389/fninf.2019.00014.

Cover T.M. & Thomas J.A. (2006). *Elements of Information Theory*. Wiley-Interscience.

De Domenico M., Solé-Ribalta A., Cozzo E., Kivelä M., Moreno Y., Porter M.A., Gómez S. and Arenas A. (2013). *Mathematical Formulation of Multilayer Networks*. Physical Review X 3 (4): 041022. https://doi.org/10.1103/PhysRevX.3.041022.

De Domenico M., Sasai S. and Arenas A. (2016). *Mapping Multiplex Hubs in Human Functional Brain Networks*. Frontiers in Neuroscience 10. https://doi.org/10.3389/fnins.2016.00326.

De Monte V.E., Geffen G.M., Massavelli B.M. (2006). *The effects of post-traumatic amnesia on information processing following mild traumatic brain injury*. Brain Inj. https://doi.org/10.1080/02699050601082073.

Dimitriadis S.I., Laskaris N.A., Micheloyannis S. (2015). *Dynamics of EEG-based Network Microstates unmask developmental and task differences during mental arithmetic and resting wakefulness*. In Press in Cognitive Neurodynamics. https://doi.org/10.1007/s11571-015-9330-8.

Dimitriadis S.I., Salis C., Tarnanas I. and Linden D.E. (2017). *Topological Filtering of Dynamic Functional Brain Networks Unfolds Informative Chronnectomics: A Novel Data-Driven Thresholding Scheme Based on Orthogonal Minimal Spanning Trees (OMSTs)*. Front. Neuroinform. 11:28. https://doi.org/10.3389/fninf.2017.00028.

Fraschini M., Demuru M., Crobe A., Marrosu F., Stam C.J., Hillebrand A. (2016). *The effect of epoch length on estimated EEG functional connectivity and brain network organisation*. J Neural Eng. 13(3):036015. https://doi.org/10.1088/1741-2560/13/3/036015.

Friston, K.J. (1994), *Functional and effective connectivity in neuroimaging: A synthesis*. Hum. Brain Mapp., 2: 56-78. https://doi.org/10.1002/hbm.460020107.

Guillon J. (2018). *Multilayer Approach to Brain Connectivity in Alzheimer's Disease*. Computer science. Sorbonne Université.

Guillon J., Chavez M., Battiston F., Attal Y., La Corte V., de Schotten M.T., Dubois B., Schwartz D., Colliot O., De Vico Fallani F. (2019) *Disrupted core-periphery structure of multimodal brain networks in Alzheimer's disease*. Network Neuroscience 3 (2): 635–652. https://doi.org/10.1162/netn_a_00087.

Hämäläinen, Matti & Hari, Riitta & Ilmoniemi, Risto J. & Knuutila, Jukka & Lounasmaa, Olli V. (1993). *Magnetoencephalography—theory, instrumentation, and applications to noninvasive studies of the working human brain*. Reviews of Modern Physics. Volume 65, Issue 2. 413-497. ISSN 0034-6861 (printed). https://doi.org/10.1103/revmodphys.65.413.

Hipp J.F., Hawellek D.J., Corbetta M., Siegel M., & Engel A.K. (2012). *Large-scale cortical correlation structure of spontaneous oscillatory activity*. Nature Neuroscience, 15(6), 884-890. https://doi.org/10.1038/nn.3101.

Huang G.B. (2014). *An Insight into Extreme Learning Machines: Random Neurons, Random Features and Kernels*. Cogn Comput 6, 376–390. https://doi.org/10.1007/s12559-014-9255-2.

Huang M.X., Theilmann R.J., Robb A., Angeles A., Nichols S., Drake A., D'Andrea J., Levy M., Holland M., Song T., Ge S., Hwang E., Yoo K., Cui L., Baker D.G., Trauner D., Coimbra R., Lee R.R. (2009). *Integrated imaging approach with MEG and DTI to detect mild traumatic brain injury in military and civilian patients*. J. Neurotrauma 26, 1213–1226.

Huang M.X., Theilmann R.J., Robb A., Angeles A., Nichols S., Drake A., D'Andrea J., Levy M., Holland M., Song T., Ge S., Hwang E., Yoo K., Cui L., Baker D.G., Trauner D., Coimbra R., Lee R.R. (2009). *Integrated imaging approach with MEG and DTI to detect mild traumatic brain injury in military and civilian patients*. J. Neurotrauma 26, 1213–1226.

Huang M.X., Nichols S., Baker D.G., Robb A., Angeles A., Yurgil K.A., Drake A., Levy M., Song T., McLay R., Theilmann R.J., Diwakar M., Risbrough V.B., Ji Z., Huang C.W., Chang D.G., Harrington D.L., Muzzatti L., Canive J.M., Christopher Edgar J., Chen Y.H., Lee R.R. (2014). *Single-subject-based whole-brain MEG slow-wave imaging approach for detecting abnormality in patients with mild traumatic brain injury*. Neuroimage Clin. 5:109-19. https://doi.org/10.1016/j.nicl.2014.06.004.

Ince R.A., Giordano B.L., Kayser C., Rousselet G.A., Gross J., & Schyns P.G. (2017). *A statistical framework for neuroimaging data analysis based on mutual information estimated via a Gaussian copula*. Human Brain Mapping, 38(3), 1541-1573. https://doi.org/10.1002/hbm.23471.

Itälinna V, Kaltiainen H, Forss N, Liljeström M, Parkkonen L (2023). *Using normative modeling and machine learning for detecting mild traumatic brain injury from magnetoencephalography data*. PLOS Computational Biology 19(11): e1011613. https://doi.org/10.1371/journal.pcbi.1011613.

Jeter C.B., Hergenroeder G.W., Hylin M.J., Redell J.B., Moore A.N., Dash P.K. (2013). *Biomarkers for the diagnosis and prognosis of mild traumatic brain injury/concussion*. J. Neurotrauma 30, 657–670. https://doi.org/10.1089/neu.2012.2439

Johnston K.M., Ptito A., Chankowsky J., & Chen J.K. (2001). *New frontiers in diagnostic imaging in concussive head injury*. Clinical journal of sport medicine, 11(3), 166-175.

Kay T., Harrington D.E., Adams R., Anderson T., Berrol S., Cicerone K. et al. (1993). *Definition of mild traumatic brain injury*. J. Head Trauma Rehabil. 8, 86–87.

Khazaeea A., Ebrahimzadehb A. and Babajani-Feremi A. (2017). *Classification of patients with MCI and AD from healthy controls using directed graph measures of resting-state fMRI*. Behav. Brain Res. 322(Pt B), 339–350. https://doi.org/10.1016/j.bbr.2016.06.043.

Kirkwood M.W., Yeates K.O. & Wilson P.E. (2006). *Pediatric sport-related concussion: a review of the clinical management of an oft-neglected population*. Pediatrics, 117(4), 1359-1371.

Klepl D., He F., Wu M., Blackburn D. & Sarrigiannis P. (2022). *EEG-Based Graph Neural Network Classification of Alzheimer's Disease: An Empirical Evaluation of Functional Connectivity Methods*. IEEE Transactions on Neural Systems and Rehabilitation Engineering. PP. 1-1. https://doi.org/10.1109/TNSRE.2022.3204913.

Leahy R.M., Mosher J.C., Spencer M.E., Huang M.X., Lewine J.D. (1998) *A study of dipole localization accuracy for MEG and EEG using a human skull phantom*. Electroencephalography and Clinical Neurophysiology, 107(2), 159-173. https://doi.org/10.1016/S0013-4694(98)00057-1.

Lerman K., Teng S. & Yan X. (2016). *Network Composition from Multi-layer Data*. ArXiv, https://doi.org/abs/1609.01641.

Levin H.S. (2009). *Mission Connect Mild TBI Translational Research Consortium*. Baylor College of Medicine Houston TX.

Levin H.S., Mattis S., Ruff R.M., Eisenberg H.M., Marshall L.F., Tabaddor K., High W.M. Jr, Frankowski R.F. (1987) *Neurobehavioral outcome following minor head injury: a three-center study*. J Neurosurg. 66(2):234-43. https://doi.org/10.3171/jns.1987.66.2.0234.

Li L., Pagnotta M.F., Arakaki X., Tran T., Strickland D., Harrington M. and Zouridakis G. (2015). *Brain Activation Profiles in mTBI: Evidence from Combined Resting-State EEG and MEG Activity*, Conf Proc IEEE Eng Med Biol Soc. https://doi.org/10.1109/EMBC.2015.7319994.

Luo Q., Xu D., Roskos T., Stout J., Kull L., Cheng X., Whitson D., Boomgarden E., Gfeller J., Bucholz R.D. (2013). *Complexity analysis of resting state magnetoencephalography activity in traumatic brain injury patients*. J. Neurotrauma 30, 1702–1709. https://doi.org/10.1089/neu.2012.2679.

National Institute on Aging (2008). *Alzheimer 's disease. Unraveling the Mystery,* volume 08-3782 of the National Institute of Health (NIH) Publication. U.S. Department of Health and Human Services.

Nolte G., Bai O., Wheaton L., Mari Z., Vorbach S., Hallett M. (2004). *Identifying true brain interaction from EEG data using the imaginary part of coherency*. Clin Neurophysiol. 115(10):2292-307. https://doi.org/10.1016/j.clinph.2004.04.029.

Nunez P.L. and Srinivasan R. (2006). *Electric Fields of the Brain: The Neurophysics of EEG*. Oxford University Press, Oxford.

Oostenveld R., Fries P., Maris E., Schoffelen J.M. (2011). *FieldTrip: Open-source software for advanced analysis of MEG, EEG, and invasive electrophysiological data*. Comput Intell Neurosci. 2011:156869. https://doi.org/10.1155/2011/156869.

Palva J.M. and Palva S. (2018), *Functional integration across oscillation frequencies by cross-frequency phase synchronization*. Eur J Neurosci, 48: 2399-2406. https://doi.org/10.1111/ejn.13767.

Pasquale F., Penna S.D., Sporns O., Romani G.L. & Corbetta, M. (2016). *A Dynamic Core Network and Global Efficiency in the Resting Human Brain*. Cerebral Cortex, 26(10), 4015-4033. https://doi.org/10.1093/cercor/bhv185.

Pedersen M., Omidvarnia A., Walz J.M., Zalesky A., Jackson G.D. (2017). *Spontaneous brain network activity: Analysis of its temporal complexity*. Network Neuroscience, 1(2),100–115. https://doi.org/10.1162/netn_a_00006.

Raskin S.A. (2000). *Memory*. In: Raskin, S.A., Mateer, C.A. (Eds.), *Neuropsychological Management of Mild Traumatic Brain Injury*. Oxford University Press, New York, 93–107.

Rohling M.L., Binder L.M., Demakis G.J., Larrabee G.J., Ploetz D.M., & Langhinrichsen-Rohling J. (2011). *A meta-analysis of neuropsychological outcome after mild traumatic brain injury: Re-analyses and reconsiderations of Binder et al. (1997), Frencham et al. (2005), and Pertab et al. (2009)*. The Clinical Neuropsychologist, *25*(4), 608–623. https://doi.org/10.1080/13854046.2011.565076.

Rubinov M., Sporns O. (2010). *Complex network measures of brain connectivity: uses and interpretations*. Neuroimage. 52(3):1059-69. https://doi.org/10.1016/j.neuroimage.2009.10.003.

Ruff R.M., Levin H.S., Mattis S., High W.M., Jr. Marshall L.F., Eisenberg, H.M. & Tabaddor, K. (1989). Recovery of memory after mild head injury: A three-center study. In H. S. Levin, H. M. Eisenberg, & A. L. Benton (Eds.), *Mild head injury* (pp. 176–188). Oxford University Press.

Sanei S. and Chambers J.A. (2007) *EEG Signal Processing*. John Wiley & Sons Ltd., 35-125. https://doi.org/10.1002/9780470511923.

Schnitzler A, Gross J. (2005). *Normal and pathological oscillatory communication in the brain*. Nat Rev Neurosci. 6(4):285-96. https://doi.org/10.1038/nrn1650.

Seenappa M.G. (2019) *Graph Classification using Machine Learning Algorithms*. Master's Projects. 725. https://doi.org/10.31979/etd.b9pm-wpng.

Siegel J.S., Shulman G.L., Corbetta M. (2017). *Measuring functional connectivity in stroke: Approaches and considerations*. Journal of Cerebral Blood Flow & Metabolism. 37(8):2665-2678. https://doi.org/10.1177/0271678X17709198.

Sigurdardottir S., Andelic N., Roe C., Jerstad T., Schanke A.K. (2009). *Post-concussion symptoms after traumatic brain injury at 3 and 12 months post-injury: a prospective study*. Brain Inj. https://doi.org/10.1080/02699050902926309.

Song J., Nair Veena A., Wolfgang G., and Vivek P. (2015). *Disrupted brain functional organization in epilepsy revealed by graph theory analysis*. Brain Connec. 5, 276–283. https://doi.org/10.1089/brain.2014.0308.

Supekar K., Menon V., Rubin D., Musen M., Greicius M.D. (2008). *Network analysis of intrinsic functional brain connectivity in Alzheimer's disease*. PLoS Comput Biol. 4(6): e1000100. https://doi.org/10.1371/journal.pcbi.1000100.

Tewarie P., Schoonheim M.M., Schouten D.I., Polman C.H., Balk L.J., Uitdehaag B.M.J. et al. (2015). *Functional brain networks: linking thalamic atrophy to clinical disability in multiple sclerosis, a multimodal fMRI and MEG Study*. Hum. Brain Mapp. 36, 603–618. https://doi.org/10.1002/hbm.22650.

Tsirka V., Simos P.G., Vakis A., Kanatsouli K., Vourkas M., Erimaki S., Pachou E., Stam C.J., Micheloyannis S. (2011). *Mild traumatic brain injury: Graph-model characterization of brain networks for episodic memory*. Int. J. of Psychophysiol. 79, 89–96. https://doi.org/10.1016/j.ijpsycho.2010.09.006.

Vanderploeg R.D., Curtiss G., Belanger H.G. (2005). *Long-term neuropsychological outcomes following mild traumatic brain injury*. J Int Neuropsychol Soc. https://doi.org/10.1017/S1355617705050289.

Varela F., Lachaux J.P., Rodriguez E. et al. (2001). *The brainweb: Phase synchronization and large-scale integration*. Nat Rev Neurosci **2**, 229–239. https://doi.org/10.1038/35067550.

Velmurugan J., Sinha S., Satishchandra P. (2014). Magnetoencephalography recording and analysis. Ann Indian Acad Neurol. 17(Suppl 1): S113-9. https://doi.org/10.4103/0972-2327.128678.

Watts D., Strogatz S. (1998). *Collective dynamics of 'small world' networks*. Nature **393**, 440–442. https://doi.org/10.1038/30918.

Zouridakis G., Paditar U., Situ N., Rezaie R., Castillo E., Levin H., Papanicolaou A.C. (2012). *Functional Connectivity Changes in Mild Traumatic Brain Injury Assessed Using Magnetoencephalography*. J of Mechanics in Medicine and Biology 12(02). https://doi.org/10.1016/j.nicl.2015.09.011.